Chem Soc Rev

REVIEW ARTICLE

View Article Online
View Journal | View Issue

Check for updates

Cite this: *Chem. Soc. Rev.*, 2019, 48, 1596

Critical review of the molecular design progress in non-fullerene electron acceptors towards commercially viable organic solar cells†

Andrew Wadsworth, *[a] Maximilian Moser,[a] Adam Marks,[a] Mark S. Little,[a] Nicola Gasparini,[bc] Christoph J. Brabec,[bd] Derya Baran[c] and Iain McCulloch[ac]

Received 21st December 2017

DOI: 10.1039/c7cs00892a

rsc.li/chem-soc-rev

Fullerenes have formed an integral part of high performance organic solar cells over the last 20 years, however their inherent limitations in terms of synthetic flexibility, cost and stability have acted as a motivation to develop replacements; the so-called non-fullerene electron acceptors. A rapid evolution of such materials has taken place over the last few years, yielding a number of promising candidates that can exceed the device performance of fullerenes and provide opportunities to improve upon the stability and processability of organic solar cells. In this review we explore the structure–property relationships of a library of non-fullerene acceptors, highlighting the important chemical modifications that have led to progress in the field and provide an outlook for future innovations in electron acceptors for use in organic photovoltaics.

Open Access Article. Published on 26 April 2018. Downloaded on 3/28/2024 5:48:32 PM.
This article is licensed under a Creative Commons Attribution 3.0 Unported Licence.

1. Introduction

Fullerene-based acceptors, such as phenyl-C_{60}-butyric acid methyl ester ($PC_{60}BM$), its C_{70} analogue ($PC_{70}BM$) and indene-C_{60} bisadduct (ICBA), have long been the dominant electron accepting materials used in bulk heterojunction solar cells; with promising results being obtained when these acceptors are used in combination with low-bandgap electron donating polymers. Despite their success, however, many problems and limitations still persist in organic solar cells that cannot be addressed without replacing this aging class of acceptors. The emergence of alternatives to fullerene-based electron acceptors has revitalized the field of organic photovoltaics (OPVs) somewhat over the past few years.

Fullerenes possess a number of advantageous properties, allowing them to produce highly efficient solar cells and their initial success in the field of organic photovoltaics. Many of the properties that have allowed fullerene acceptors to excel are derived from the 3D-conjugated cage structure inherent to these molecules. For example, the lowest unoccupied molecular orbitals (LUMOs) of the fullerene acceptors are delocalized across the entire 3D surface of the C_{60} or C_{70} cages, allowing efficient and isotropic electron transport.[1] This delocalisation of the molecular orbitals across the 3D fullerene cages also provides the acceptors with the ability to undergo weak π–π interactions, such that small scale aggregation of the fullerene acceptors can occur forming nanoscale pure and mixed domains in the bulk heterojunction.[2] The formation of domains on the lengthscale of the exciton diffusion length (5–15 nm for organic semiconductor blends) is necessary for efficient exciton splitting and free charge generation in active layer blends.[3,4]

However, the same 3D cage structures are responsible for some of the most significant drawbacks of fullerene acceptors. The highly symmetric nature of the wavefunctions render the optical transitions forbidden, impeding the ability of the fullerenes to absorb photons in the UV-visible region of the solar spectrum, thereby limiting the contribution of the acceptor towards the photogenerated current of the solar cells and condemning them to rely mainly on p-type (Channel-I) excitation. $PC_{70}BM$ was designed to overcome this issue; the lower symmetry of the C_{70} cages leads to a greater number of allowed optical transitions within the molecule, enhancing the ability of the acceptor to harvest photons. It must be noted that this is still dramatically lower in intensity than the absorption of the donor polymer in the UV-visible region of the solar spectrum, and thus Channel-I

[a] Department of Chemistry and Centre for Plastic Electronics, Imperial College London, London, SW7 2AZ, UK. E-mail: andrew.wadsworth11@imperial.ac.uk
[b] Institute of Materials for Electronics and Energy Technology (I-MEET), Friedrich-Alexander-University Erlangen-Nuremberg, Martensstraße 7, 91058 Erlangen, Germany
[c] Physical Sciences and Engineering Division, KAUST Solar Center (KSC), King Abdullah University of Science and Technology (KAUST), KSC Thuwal 23955-6900, Saudi Arabia
[d] Bavarian Center for Applied Energy Research (ZAE Bayern), Haberstrasse 2a, 91058 Erlangen, Germany

† Electronic supplementary information (ESI) available. See DOI: 10.1039/c7cs00892a

This journal is © The Royal Society of Chemistry 2019

Open Access Article. Published on 26 April 2018. Downloaded on 3/28/2024 5:48:32 PM.
This article is licensed under a Creative Commons Attribution 3.0 Unported Licence.

excitation is still mainly predominant.[5] The delocalisation of the LUMO across the 3D cages also presents an issue for the fullerene acceptors, whereby it is difficult to chemically modify the LUMO by the inclusion of additional functional groups on the C_{60} cage. There have been some successful attempts to shift the LUMO level of the acceptors by the addition of functional groups, such as methano- and diphenyl methano-adducts, or the inclusion of amines or fluorine atoms on the phenyl unit of the adduct, however only small shifts (<0.2 eV) have been reported, with poorer synthetic yields.[6–9] The inability to alter the frontier molecular orbitals (FMOs) results in poor tunability of the absorption spectrum of these acceptors, and hence limits the photocurrent that can be produced in the bulk heterojunction. Additionally, the open circuit voltage (V_{OC}) achieved in organic solar cells has been shown to display a dependence on the difference in energy between the highest occupied molecular orbital (HOMO) of the donor and the LUMO of the acceptor. Therefore, the ability to tune the LUMO of the acceptor is critical to maximizing the V_{OC} that an organic solar cell can achieve, and this is not straightforward when using fullerene based acceptors. The strong tendency of fullerenes to aggregate can cause long-term morphological stability issues in fullerene-containing solar cells. Whilst the aggregation of the acceptors can be favourable up to a point, aiding in the formation of the correct morphology in the bulk heterojunction in the short-term, this aggregation continues after the active layer has been cast; leading to microscale aggregates forming over time in the blend.[10] These large aggregates that form over time are far larger than the exciton diffusion length leading to significant exciton relaxation and recombination of free charge carriers in the blends. In an operational solar cell, fullerene acceptors have also been shown to migrate to the device's anode over time, this eventually leads to delamination of the device, rendering it inoperational.[11] Additionally, the relatively poor solubility of fullerenes, a result of their strong tendency to aggregate, can also be problematic in the short-term. Without the use of high-boiling additives such as 1,8-diiodooctane (DIO) and 1-chloronaphthalene (CN), fullerene acceptors tend to form microscale domains and aggregates. However the use of these halogenated additives has been shown to be detrimental to the long-term photostability of active layers.[12] Therefore, eliminating the need for these additives is necessary to produce photo- and morphologically stable organic solar cells.

Despite the rather significant shortcomings of the fullerene based acceptors, they have remained prevalent in the field of organic solar cells owing to their favourable electron accepting and transport properties, which have been difficult to replicate, and practically, their ready availability from a range of chemical suppliers. In lieu of replacing the fullerene acceptors, there has been a focus on improving solar cell performance through the rational design of the donor polymers and strategic device engineering over the past several years.[13] As stated above, the relatively weak absorption of the fullerene acceptors in the UV-visible region limits most fullerene containing solar cells to Channel-I excitation, where the donor polymer is largely responsible for exciton generation, therefore low-bandgap donor polymers with broad absorption were developed in order to improve the photocurrent that could be achieved, since they are able to absorb light of longer wavelengths. Push–pull copolymers are able to achieve low bandgaps by making use of molecular orbital hybridization of electron rich and electron poor units in the conjugated polymer backbone, which effectively reduces the bandgap. Polymers such as PTB7-Th and PffBT4T-2OD make use of push–pull hybridization to achieve long wavelength light absorption, in addition to high hole mobility and favourable aggregation properties, to produce solar cells that were able to achieve power conversion efficiencies (PCEs) exceeding 10 and 11% respectively, when used in combination with fullerene acceptors.[14,15] Another approach to improve the photon harvesting capabilities of the active layer is by employing a ternary system, whereby a third organic semiconductor is added to the active layer. The inclusion of a second donor polymer, which predominantly absorbs in a different region of the spectrum to the other donor polymer, allows a greater fraction of photons to be absorbed, and so the photocurrent can be improved.[16,17] The use of ternary systems can also provide a means of improving the V_{OC} in fullerene-containing solar cells. If the additional polymer component has a deeper lying HOMO the V_{OC} can be raised in comparison to the corresponding binary device.[18,19] Unfortunately, ternary solar cells that contain two polymer components tend to be quite difficult to fabricate with optimal phase separation; this is a result of the unfavourable mixing of polymers due to a lack of entropic driving force. To address the poor morphological stability of fullerene-containing active layers, crosslinking has been employed to create a more robust microstructure within the active layer. Examples where the donor polymer and the fullerene acceptor have been crosslinked have both been shown successfully;[20–22] a key conclusion from these reports is that it is preferable to crosslink at a site that does not perturb the conjugated system (*i.e.* on the side chains of the materials).[23] Whilst crosslinking in the active layer has been shown to improve the morphological stability of blends, it often results in decreased PCE, an increased risk of electrode delamination and requires synthetically complex and expensive derivatives of donor polymers or fullerene acceptors.[23] Overcoming the need for high-boiling halogenated additives for effective fullerene containing bulk heterojunctions has also been addressed in a recently reported system.[24] The devices were fabricated from an entirely non-halogenated processing conditions, while still achieving a high PCE (11.7%). By replacing the high-boiling additive (DIO) with a non-halogenated equivalent, 2-phenyl naphthalene (PN), the active layer photostability should be improved.

Although the aforementioned approaches have overcome many of the issues presented by fullerenes, they bring new problems of their own into focus. A more elegant approach to address the drawbacks of fullerene acceptors is to replace them with strategically designed electron accepting materials. Non-fullerene acceptors (NFAs), which have been specifically designed to match the electron accepting and transport properties possessed by fullerenes, and also to overcome the poor optical properties and long term morphological instability associated with fullerene acceptors, provide an attractive alternative to the use of

Open Access Article. Published on 26 April 2018. Downloaded on 3/28/2024 5:48:32 PM.
This article is licensed under a Creative Commons Attribution 3.0 Unported Licence.

fullerenes and employing the other strategies mentioned above. Most NFAs, similar to donor polymers, make use of push–pull hybridisation, allowing them to absorb strongly in the visible and near IR region of the solar spectrum. As such, these acceptors are able to absorb a greater fraction of photons and consequently form excitons to be split into free charge carriers; this is n-type (Channel-II) excitation. If both the donor and the acceptor are able to absorb photons in different regions of the spectrum, the total fraction of excitons being utilized is increased and the photocurrent can be maximized. Chemical modification of these structures allow a greater degree of control over the FMOs of the acceptors, leading to a wider range of possible donor polymers to be used, and the ability to achieve a much higher V_{OC} in devices. Another common feature of NFAs is the use of steric hindrance or the inclusion of solubilising alkyl chains in order to gain some control over their aggregation properties; rendering them easier to process in common organic solvents than their fullerene counterparts. Beyond these common features, NFAs employ a wide range of novel approaches in an attempt to improve upon the standard set by fullerene acceptors. This has yielded a diverse range of exciting new materials that have already begun to push the field of organic photovoltaics to new heights (Fig. 1).

Care must be taken when comparing these acceptors across the reported literature, with a number of factors affecting the optoelectronic properties of the acceptors and the *J*–*V* characteristics of OPV devices. For example, particular caution must be used when drawing comparison between the reported energy levels of the acceptors, since there is no universal procedure for measuring them. Photo-electron spectroscopy in air (PESA) and cyclic voltammetry (CV) are both commonly employed to measure the ionization potentials (IP) and electron affinity (EA) of an organic semiconductor. However, the variety of conditions and reference values used in CV measurements can lead to quite different measured values for the same material, particularly the values used to define the vacuum level, and comparisons must therefore be made with care. In terms of *J*–*V* characteristics, there are factors that must be accounted for when comparing the performance of OPV devices, even if the same donor polymer is being used: (i) the device architecture can play a huge role in

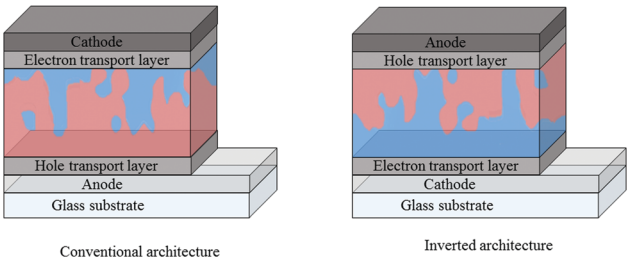

Fig. 2 Conventional and inverted architectures employed in bulk heterojunction organic solar cells, where the electron donor is denoted by red regions and the electron acceptor by blue regions.

the performance of devices – vertical phase separation in the active layer can lead to electron donor or acceptor rich layers in the blend and depending on whether one extracts the electrons from the top of the device (conventional) or the bottom (inverted), the electrons may have to travel through a donor or acceptor rich region before being extracted, affecting charge carrier mobilities and recombination rates in the bulk heterojunction,[25,26] (ii) the electron and hole transport layers (ETL and HTL respectively), can also have a significant influence on device performance – the choice of these layers can affect the ease of extraction of free charges at the contacts of the device, along with recombination and resistive losses (Fig. 2).[27–29]

In this review, we document the great strides that have been made by non-fullerene acceptors over the past few years. We discuss the main classes of NFAs and relate their molecular and device properties to the key structural characteristics of the materials. By highlighting these strategic design principles, we aim to provide a foundation for future innovation in the field and move closer towards the end goal of commercially viable large scale organic photovoltaics.

Early frontrunners in the field of non-fullerene acceptors also included subphthalocyanines (SubPCs), subnaphthalocyanines (SubNCs) and truxenones (Fig. 3). SubPCs are a subcategory of phthalocyanines, consisting of three fully conjugated diimino-isoindole moieties affording an aromatic macrocyclic structure surrounding a central boron atom. Their initial success in OPVs was closely tied to their favourable energy levels affording high V_{OC}, strong absorption coefficients, in excess of 3.5×10^5 cm^{-1}, and excellent thermal and chemical stabilities.[30–32] Subnaphthalocyanines (SubNCs), the higher homologue of SubPCs have also been developed and share their same advantageous properties. The highest PCE of binary OPV blends employing either SubPCs or

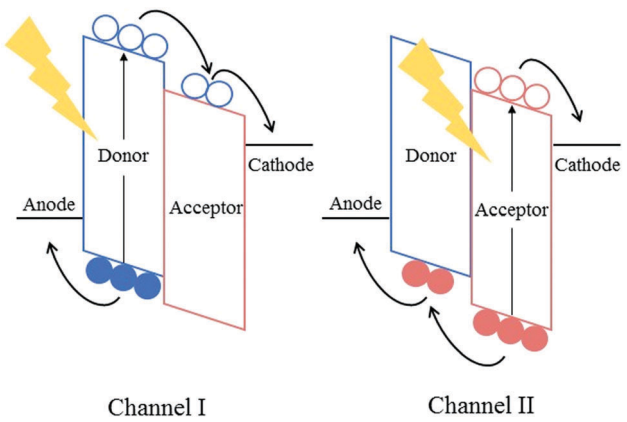

Fig. 1 Channel I and II excitation in organic solar cells.

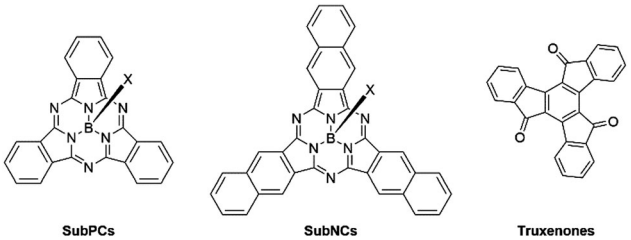

Fig. 3 General structure of SubPC, SubNC and truxenone NFAs.

This journal is © The Royal Society of Chemistry 2019

Open Access Article. Published on 26 April 2018. Downloaded on 3/28/2024 5:48:32 PM.
This article is licensed under a Creative Commons Attribution 3.0 Unported Licence.

SubNCs as electron acceptor was reported in 2015 and yielded 6.86%. Since then, additional research efforts into this class of NFAs were unable to eclipse this benchmark. Another drawback of SubPCs and SubNCs is their more energy and capital expensive vacuum-processing, thus also contributing to their decline. Similar to SubPCs, truxenones were another type of rotationally symmetrical vacuum-deposited small molecule NFAs, characterised by their easily tuneable molecular curvature and in turn their optoelectronic and morphological properties. Truxenones' inherently low crystallisation tendency often resulted in poor charge transport properties thus severely limiting the FF of devices. Consequently, the PCEs of donor:truxenone systems were never able to exceed 3%.[33–35]

2. Acceptor–donor–acceptor calamitic small molecules

Despite being a relatively new class of electron acceptors, acceptor–donor–acceptor (A–D–A) calamitic-type small molecules appear to be among the most promising replacements for fullerenes to have been reported, with PCEs now exceeding 11% being achieved regularly. Their classification as A–D–A type acceptors is derived from their generic structure of an electron rich donor central core flanked on either side by electron deficient acceptor units. They have been designed in a modular fashion, hence tuning the FMOs and absorption spectra can be easily and readily achieved by substituting one electron donating (or electron withdrawing) unit with another. The LUMO of these molecules is mostly located on the electron withdrawing (acceptor) units on the periphery of the molecule, and the HOMO is mainly located on the electron rich (donor) core. As such, any structural changes on the periphery have a much greater effect on the LUMO than the HOMO, and alterations to the donor core have a greater impact on the HOMO of the acceptor, allowing independent control over both the HOMO and LUMO levels. Another advantage of these A–D–A small molecules, in comparison to the extended rigid fused ring acceptors, is the relative ease with which they can be synthesized. Also, like all small molecules, these A–D–A type acceptors do not suffer from the batch-to-batch variations in molecular weight, polydispersity and purity that is regularly seen in polymers.

Fluorene, carbazole, indaceno[1,2-*b*:5,6-*b*′]dithiophene (IDT), indacenodithieno[3,2-*b*]thiophene (IDTT), and their derivatives, are the most commonly used donor units in the core of these molecules, and established dye based moieties, such as diketopyrrolopyrrole (DPP), indandione and rhodanine derivatives, are most commonly used on the electron withdrawing periphery of the molecules. The main differences between many of these acceptors lies within the π-conjugated spacer unit (if one is included at all) between the donor unit in the core and acceptor units, allowing further tuning of the HOMO, LUMO and bandgap. Chemical modifications to the dye based end groups are also commonly employed to easily tune the optoelectronic and structural properties of these acceptors.

2.1. Fluorene and carbazole based acceptors

The fluorene moiety was among the first to be used as the donor unit in A–D–A type NFAs, owing to its simple synthesis and ready availability, in addition to the facile inclusion of solubilizing chains allowing a degree of control over structural properties (Fig. 4). One of the first examples of such an NFA was reported in 2014, where alkylated carbazole and fluorene cores were flanked by thiophenes and 3-ethylrhodanine end groups to create **Cz-RH** and **Flu-RH** respectively (Table 1).[36] These acceptors possessed high lying LUMOs (approx. −3.5 eV), to aid in maximizing the V_{OC}, which was achieved with the use of an electron donating thiophene spacer unit. Another important feature of the thiophene spacer was to ensure that the acceptor was planar. Where phenyl–phenyl links are used, the molecular backbone tends to twist to avoid the steric clash of ortho-hydrogens. However, in phenyl–thienyl links, this steric strain is much less as the ortho-hydrogens are much further from one another, hence the molecular backbone no longer has to twist to avoid steric strain. When used in combination with P3HT, **Cz-RH** and **Flu-RH** were able to achieve PCEs of 2.56% and 3.08% respectively, where the high V_{OC} (1.03 V for both acceptors) played a large role in the success of these NFAs. The main limitation of the solar cell performance was modest J_{SC}, which can be partly attributed to the fact that the NFAs absorb in the same region of the solar spectrum as P3HT (E_g = 2.10 eV), limiting the fractions of photons that can be harvested in this system. This design concept was then developed further with the acceptor, **F(DPP)$_2$B$_2$**.[37] Again, this acceptor utilized an alkylated fluorene as the electron donating core, and contained thiophene spacer groups, but was flanked by alkylated diketopyrrolopyrrole (DPP) moieties on the periphery of the molecule. Strongly electron withdrawing DPP units were employed to narrow the bandgap of the acceptor (E_g = 1.82 eV), such that complimentary absorption could be achieved. Using P3HT as the donor material, solar cells were able to achieve an exceptionally high V_{OC} of 1.18 V, owing to the high lying LUMO (−3.4 eV), however the J_{SC} and fill factor (FF) could not be improved upon, relative to **Flu-RH** and **Cz-RH** containing devices. This design was also utilized as a basis to develop **FBR**.[38] Again, it contained the alkylated fluorene donor as the core, but was this time flanked by electron withdrawing benzothiadiazole (BT) and 3-ethylrhodanine units on the periphery. Whilst the increased electron withdrawing character on the molecule should theoretically serve to narrow the bandgap, this is mitigated by the phenyl–phenyl link between the fluorene and BT units. Geometry optimization calculations, using Density Functional Theory (DFT), estimated a ∼35° twist in the backbone (using B3LYP/6-31G* level) to avoid the steric clash of ortho-hydrogen atoms, as discussed above, and thus yielding a wide bandgap of 2.14 eV. The inclusion of the strongly electron withdrawing BT spacer served to lower the LUMO level of the acceptor to −3.6 eV, which would thereby lead to a decrease in the V_{OC} relative to the aforementioned acceptors. Solar cells using P3HT as the donor were able to achieve a V_{OC} of 0.82 V, but much improved J_{SC} and FF (7.95 mA cm^{-2} and 0.63 respectively), which can be attributed to the use of an inverted

Open Access Article. Published on 26 April 2018. Downloaded on 3/28/2024 5:48:32 PM.
This article is licensed under a Creative Commons Attribution 3.0 Unported Licence.

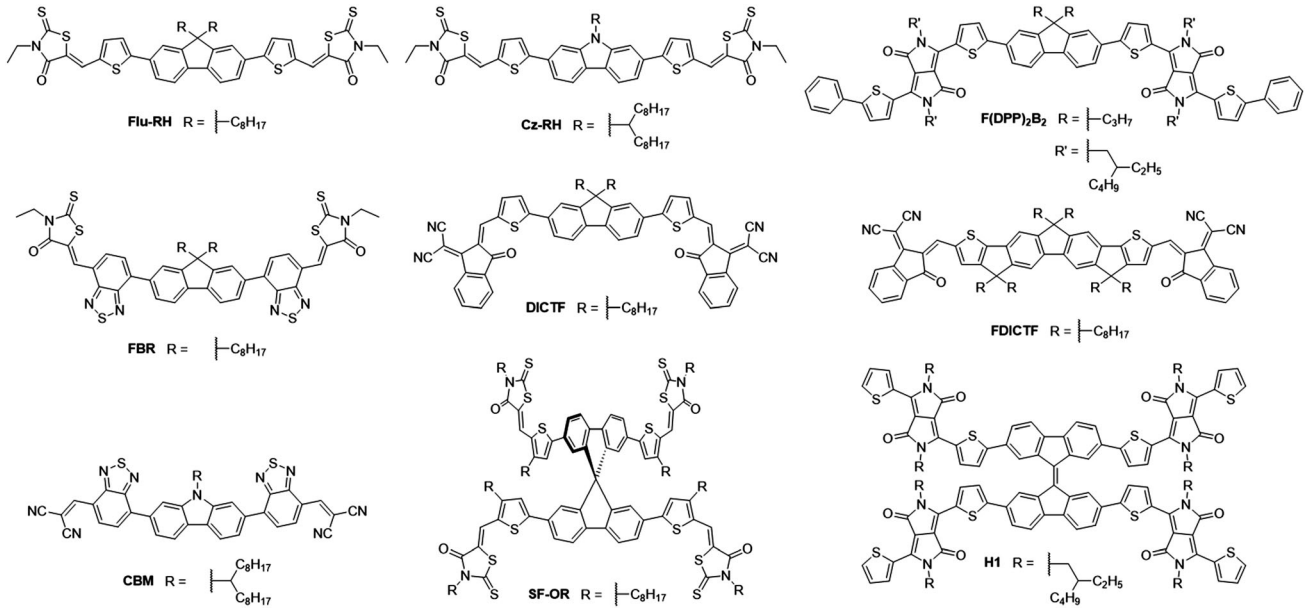

Fig. 4 Fluorene and carbazole based small molecule A–D–A type acceptors.

Table 1 Summary of the optoelectronic properties of fluorene and carbazole based small molecule A–D–A type acceptors and their *J*–*V* characteristics in bulk heterojunction solar cells

Acceptor	Optical E_g (eV)	HOMO (eV)	LUMO (eV)	V_{OC} (V)	J_{SC} (mA cm^{-2})	FF	Electron mobility[a] (cm^2 V^{-1} s^{-1})	Hole mobility[b] (cm^2 V^{-1} s^{-1})	PCE[c] (%)	Donor	Additive	Ref.
Cz-RH	2.05	−3.50	−5.53	1.03	4.69	0.53	—	—	2.56 (—)	P3HT	—	36
Flu-RH	2.10	−3.53	−5.58	1.03	5.70	0.52	—	—	3.08 (—)	P3HT	—	36
F(DPP)$_2$B$_2$	1.82	−3.39	−5.21	1.18	5.35	0.50	2.80×10^{-4}	4.30×10^{-5}	3.17 (—)	P3HT	—	37
FBR	2.14	−3.57	−5.70	0.82	7.95	0.63	2.60×10^{-5}	—	4.11 (—)	P3HT	—	38
FBR	2.14	−3.57	−5.70	1.13	11.70	0.63	3.80×10^{-4}	—	8.00 (7.80)	PffBT4T-2DT	—	39
DICTF	1.82	−3.79	−5.67	0.86	16.61	0.56	1.93×10^{-4}	3.82×10^{-4}	7.93 (7.63)	PTB7-Th	—	40
FDICTF	1.63	−3.71	−5.43	0.95	16.09	0.67	2.40×10^{-5}	3.37×10^{-5}	10.06 (9.81)	PBDB-T	—	41
CBM	2.02	−4.13	−6.05	0.88	10.60	0.53	1.90×10^{-6}	1.00×10^{-4}	5.30 (5.00)	PTB7-Th	2.0% DIO	42
SF-OR	2.15	−3.25	−5.50	0.97	7.50	0.65	6.71×10^{-6}	8.49×10^{-5}	4.70 (4.46)	P3HT	—	43
H1	1.67	−3.84	−5.51	1.17	7.74	0.60	2.40×10^{-3}	—	5.40 (—)	P3HT	—	44

[a] Determined by space charge limited current (SCLC) measurements using electron only devices. [b] Determined by space charge limited current (SCLC) measurements using hole only devices. [c] Average PCE values are shown in parentheses.

device architecture rather than a conventional architecture, in addition to the improved electron accepting abilities of this molecule. Overall this led to an impressive PCE of 4.1%. However, it was found that the device was limited by two major factors: (i) the very similar absorption spectra of **FBR** and P3HT, limiting the photocurrent that could be achieved, (ii) the amorphous nature of the acceptor, owing to its twisted structure, which led to it becoming molecularly mixed with the P3HT. As a result of the molecular mixing, the acceptor was unable to aggregate to form the nanoscale domains and percolating networks needed for efficient exciton separation and extraction of free charges in the blend, and thus large nongeminate recombinative losses were observed in the system. Good morphological stability under extended thermal annealing was demonstrated, where the acceptor did not form large aggregates, which is often seen in fullerene containing devices. When **FBR** was later combined with the low bandgap donor polymer PffBT4T-2DT, it was able to achieve a PCE of 8.00%.[39] The improved PCE when **FBR** was used in combination with the low bandgap polymer can be traced back to a great improvement in both the V_{OC} and J_{SC} in devices (1.13 V and 11.7 mA cm^{-2} respectively). The increase in V_{OC} is a result of the lower lying HOMO level of PffBT4T-2DT, in comparison to P3HT, and the increase in photocurrent can be attributed to the complimentary absorption of the donor and acceptor leading to greater spectral coverage by the active layer blend. **DICTF** is another NFA that has built upon the structure of **Flu-RH**, but instead of replacing the thiophene spacer, the rhodanine end group had been replaced with a modified indandione derivative, 2-(2,3-dihydro-3-oxo-1*H*-inden-1-ylidene) propanedinitrile, often referred to as a dicyanovinylindanone (DCI) group.[40] The logic behind this strategy was to keep the molecule synthetically simple and inexpensive, by retaining the fluorene donor unit in the core, whilst attempting to lower the bandgap, which is usually relatively wide (>2.0 eV) in fluorene based acceptors. This strategy was effective in decreasing the bandgap to 1.82 eV, among the lowest with fluorene core units, by pushing the LUMO

Open Access Article. Published on 26 April 2018. Downloaded on 3/28/2024 5:48:32 PM. This article is licensed under a Creative Commons Attribution 3.0 Unported Licence.

deeper. From grazing incidence wide-angle X-ray scattering (GIWAXS) measurements, it was shown that **DICTF** displayed a preference to π-stack in a face-on orientation. When combined with PTB7-Th, a low bandgap polymer that also tends to display face-on π-stacking, the resultant OPV devices were able to achieve a substantially larger J_{SC} than any other fluorene based NFAs (16.6 mA cm^{-2}). Reasonably high and balanced charge carrier mobilities were observed in the blend ($\mu_e = 1.93 \times 10^{-4}$ cm^2 V^{-1} s^{-1} and $\mu_h = 3.82 \times 10^{-4}$ cm^2 V^{-1} s^{-1}), and along with much stronger absorption by this medium bandgap acceptor, are likely to be the cause of this particularly high photocurrent. Because **DICTF** has a relatively deep LUMO, a modest V_{OC} of 0.86 V was achieved, however the impressive J_{SC} resulted in a PCE of 7.93%. This acceptor was later improved upon by using a fluorene-based core that includes extended conjugation by fusing the thiophene spacers to the fluorene, affording **FDICTF**.[41] In fusing these units together, greater planarization and thus a greater degree of conjugation along the molecular backbone was possible; this led to a narrowing of the bandgap to 1.62 eV and the extinction coefficient was almost three times as large as that of **DICTF**. This increased conjugation also led to a change in the energy of the FMOs; with the LUMO being raised slightly (~0.1 eV), and the HOMO being raised more significantly (~0.3 eV). Due to the red-shift in absorption spectrum, relative to **DICTF**, the donor polymer that was chosen to blend with **FDICTF** was the medium bandgap PBDB-T, in order to ensure complimentary absorption profiles between the donor and acceptor. The OPV devices using this blend are among the highest that use fluorene-based acceptor molecules, attaining a PCE of 10.06%. Excellent photon harvesting and good matching of the energy levels afforded a satisfactory V_{OC} and J_{SC} to be achieved, 0.95 V and 16.09 mA cm^{-2} respectively. An impressive FF of 0.67 was achieved; with a greater degree of phase separation in the active layer. The stronger tendency to aggregate possessed by the more planar **FDICTF** is likely to have facilitated the formation of phase separated donor and acceptor domains, whereas no clear domains were seen in **DICTF** blends. Fusing adjacent conjugated units together has proven effective in lowering the bandgap of the acceptor and increasing its tendency to aggregate and phase separate from the donor polymer, resulting in improved photovoltaic performance in blends. However the added synthetic complexity associated with this strategy could be problematic in the potential scale-up of such an acceptor.

The basic design principles of fluorene containing A–D–A molecules was expanded by synthesizing a series of NFAs using electron rich central units (fluorene, carbazole and cyclopentadithiophene) flanked by benzothiadiazole units. However, the 3-ethylrhodanine groups were replaced by dicyanovinyl (DCV) moieties on the periphery; a strategy that has previously been used in the design of small molecule donor materials.[42] The reasoning for the use of DCV end groups was to promote planarity, through favourable π–π interactions, with the aim of improving the charge carrier mobility of the acceptors. **CBM**, the carbazole containing acceptor, was able to achieve the best performance of the series with a PCE of 5.3% with the low bandgap polymer PTB7-Th. Though the photocurrent was reasonably high, the devices suffered from a lower V_{OC}, especially when considering the low lying HOMO of PTB7-Th, due to the deeper LUMOs achieved in the acceptors when the DCV units are included. Additionally, these devices suffered from low FF (0.53), which also limits their performance; this is likely to be a result of an unfavourable morphology in the blends.

SF-OR, a spirobifluorene derivative of **Flu-RH** made use of a 3D structure and inherent twisting to improve upon the performance and properties of the early A–D–A type acceptors.[43] The twisted 3D structure was adopted to suppress the crystallinity and aggregation of the acceptor, acting as a method to ensure domains are on the order of the nanoscale (13.3 and 9.6 nm for donor and acceptor domains respectively). The optoelectronic properties of this acceptor are very similar to those of **Flu-RH**, with comparable FMOs and bandgap, this is because the 90° twist in the spirobifluorene unit (predicted by geometry optimization based on DFT at B3LYP/6-31G* level) acts to break the conjugation, forming what is essentially two **Flu-RH** molecules attached at the fluorene bridge. As such, **SF-OR** devices, employing P3HT as the donor polymer, exhibited a similar V_{OC} (0.97 V) to the **Flu-RH** devices. However, the J_{SC} and FF showed significant improvement (7.5 mA cm^{-2} and 0.65 respectively). The 3D structure of **SF-OR** was shown to inhibit micrometer-scale aggregation in the blend, leading to an interpenetrating donor:acceptor network on the correct length-scale. **H1** is another acceptor that makes use of a bifluorene type donor moiety at its core, this time a bifluorenylidene.[44] The bifluorenylidene moiety was attached to four thiophene-flanked diketopyrrolopyrrole (DPP) units, affording an 'H shaped' NFA. The planarity of each DPP–fluorene–DPP section of the acceptor can be attributed to the phenyl–thienyl links between the bifluorenylidene and DPP units, and in combination with the strongly electron-withdrawing character of the DPP units, **H1** was able to achieve a reasonably narrow bandgap of 1.67 eV and a low lying LUMO. The highly twisted double bond (calculated to be 40° using DFT at B3LYP/6-311G(d,p)) that links the fluorene units together acts to suppress the excessive aggregation, often seen in highly planar acceptors, and also improve the NFA's ability to accept electrons. Upon accepting an electron, a radical anion forms, which can be stabilized effectively. The anion is stabilized by one of the fluorene units, and the radical is stabilized by the other. When blended with P3HT, **H1** was able to achieve an impressive V_{OC} of 1.17 V, however could only exhibit a modest J_{SC} and FF (7.74 mA cm^{-2} and 0.60). This led to an overall PCE of 5.42%, which is among the best efficiencies achieved with P3HT as the donor polymer. Considering the low bandgap of **H1**, one would expect that the complimentary absorption of the donor polymer and NFA would lead to a high photocurrent in devices. However, this was not achieved in devices and is the parameter that limited the PCE. The low photocurrent is likely to be a result of a large amount of non-geminate recombination in the blend, caused by an intimately mixed donor:acceptor morphology; a result of the twisted nature of the acceptor.

2.2. Indacenodithiophene and indacenodithienothiophene based acceptors

Despite the early success of fluorene and carbazole based A–D–A type NFAs, it became apparent that more strongly absorbing, narrow bandgap, acceptors were desirable, particularly for

Open Access Article. Published on 26 April 2018. Downloaded on 3/28/2024 5:48:32 PM.
This article is licensed under a Creative Commons Attribution 3.0 Unported Licence.

complementary absorption when using scalable medium bandgap donor polymers such as P3HT. Many of the fluorene based acceptors also suffered from sub-optimal morphologies as a result of intimate mixing in the active layer blends, limiting the FF and photocurrent that could be achieved. With this is mind, more electron donating and planar units were identified to be used in the core of A–D–A type molecules to create narrow bandgap NFAs with enhanced self-aggregation properties. IDT and its derivatives emerged as strong candidates and have subsequently been used extensively in A–D–A type acceptors, owing to the strong electron donating and planar structures that these units possess, the relatively straightforward synthesis and good stability of these units, compared to benzodithiophene (BDT) and other typical donor moieties employed in push–pull copolymers (Fig. 5).

IEIC, an acceptor containing the IDT core flanked by thiophene spacer units and DCI end groups, was among the first A–D–A acceptors to incorporate the IDT unit at its core, in 2014.[45] This molecule can be considered as analogous to **DICTF** with the difference being the replacement of the fluorene unit at the core with IDT and using phenylhexyl solubilizing chains. The stronger electron donating character, and added planarity associated with thiophene–thiophene links, led to **IEIC** being able to achieve a bandgap of 1.57 eV. By reducing the twisting in the molecule, the effective conjugation was increased, thereby narrowing the bandgap. Also, the greater overlap of HOMO and LUMO spatial distribution improves the oscillator strength of the acceptor, increasing the absorption coefficient of **IEIC**, compared to the values previously seen in many of the fluorene containing A–D–A type acceptors. Devices were fabricated using PTB7-Th as the donor material, despite the similar absorption profiles of the donor and acceptor. A result of this poor spectral coverage was a modest J_{SC} of 13.55 mA cm^{-2}. A relatively poor FF of 0.48 was

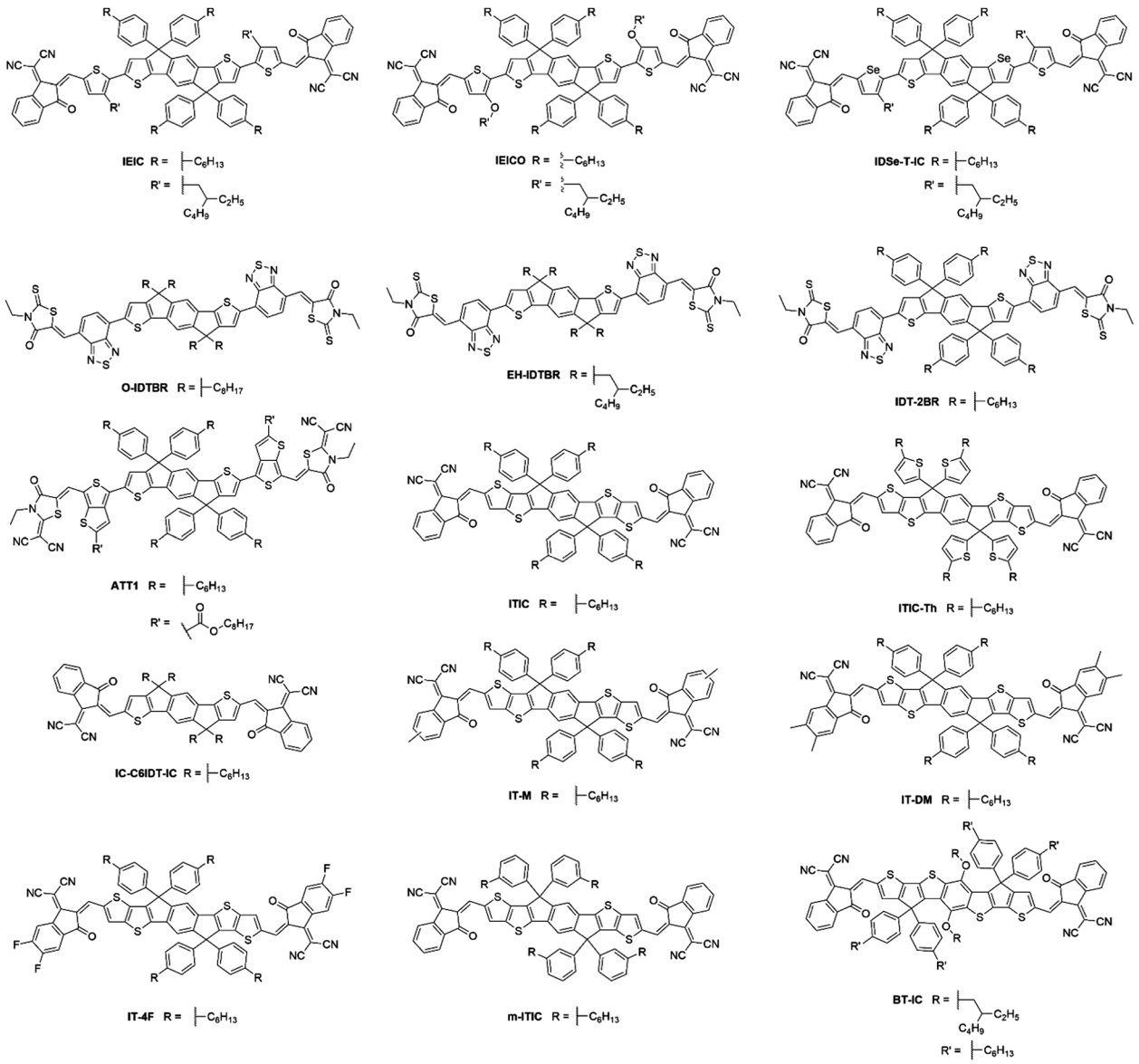

Fig. 5 IDT and IDTT based small molecule A–D–A type acceptors.

Open Access Article. Published on 26 April 2018. Downloaded on 3/28/2024 5:48:32 PM. This article is licensed under a Creative Commons Attribution 3.0 Unported Licence.

Table 2 Summary of the optoelectronic properties of IDT and IDTT based small molecule A–D–A type acceptors and their *J*–*V* characteristics in bulk heterojunction solar cells

Acceptor	Optical E_g (eV)	HOMO (eV)	LUMO (eV)	V_{OC} (V)	J_{SC} (mA cm^{-2})	FF	Electron mobility[a] (cm^2 V^{-1} s^{-1})	Hole mobility[b] (cm^2 V^{-1} s^{-1})	PCE[c] (%)	Donor	Additive	Ref.
IEIC	1.57	−3.82	−5.42	0.97	13.55	0.48	1.00×10^{-4}	4.50×10^{-4}	6.31 (6.08)	PTB7-Th	—	45
IEIC	1.57	−3.82	−5.42	1.00	12.70	0.62	2.10×10^{-4}	1.90×10^{-4}	7.30 (7.20)	PffT2-FTAZ-2DT	—	46
IEICO	1.34	−3.95	−5.32	0.82	17.70	0.58	4.60×10^{-4}	1.50×10^{-3}	8.40 (8.30)	PBDTTT-E-T	—	47
IDSe-T-IC	1.52	−3.79	−5.45	0.91	15.20	0.62	7.72×10^{-5}	8.25×10^{-5}	8.58 (8.21)	J51	—	48
O-IDTBR	1.63	−3.88	−5.51	0.73	14.10	0.62	4.70×10^{-6}	—	6.38 (6.30)	P3HT	—	49
O-IDTBR	1.63	−3.88	−5.51	0.83	14.70	0.65	3.40×10^{-6}	—	7.80 (—)	P3HT	—	50
EH-IDTBR	1.68	−3.90	−5.58	0.76	12.10	0.62	6.10×10^{-6}	6.80×10^{-4}	6.05 (—)	P3HT	—	49
EH-IDTBR	1.68	−3.90	−5.58	1.02	17.20	0.63	—	—	11.09 (10.70)	PffBT4T-2DT	—	51
IDT-2BR	1.68	−3.69	−5.52	0.84	8.91	0.68	2.00×10^{-4}	2.60×10^{-4}	5.12 (5.04)	P3HT	3.0% CN	52
IDT-2BR	1.68	−3.69	−5.52	1.02	13.90	0.60	1.70×10^{-4}	6.70×10^{-4}	7.70 (7.60)	PTB7-Th	—	53
IDT-2BR1	1.61	−3.67	−5.37	0.95	15.20	0.60	3.90×10^{-4}	1.50×10^{-4}	8.70 (8.60)	PTB7-Th	3.0% CN	54
ATT-1	1.54	−3.63	−5.50	0.87	16.48	0.70	2.40×10^{-4}	5.13×10^{-4}	10.07 (9.89)	PTB7-Th	1.0% DIO	55
ITIC	1.59	−3.78	−5.51	0.81	14.21	0.59	1.10×10^{-4}	4.30×10^{-5}	6.80 (6.58)	PTB7-Th	—	56
ITIC	1.59	−3.78	−5.51	0.95	17.87	0.67	1.00×10^{-3}	1.00×10^{-3}	11.34 (11.03)	PBQ-4F	5.0% IPA	57
ITIC	1.59	−3.78	−5.51	0.90	16.81	0.74	—	—	11.21 (10.68)	PBDB-T	0.5% DIO	64
ITIC-Th	1.60	−3.93	−5.66	0.88	16.24	0.67	6.10×10^{-4}	3.00×10^{-4}	9.60 (9.30)	PDBT-T1	1.0% CN	58
ITIC-Th	1.60	−3.93	−5.66	0.93	17.60	0.69	—	—	10.88 (10.50)	PTFB-O	—	60
IC-C6IDT-IC	1.62	−3.91	−5.69	0.89	15.05	0.65	2.90×10^{-4}	5.10×10^{-5}	8.71 (8.57)	PBDB-T	—	61
IT-M	1.60	−3.98	−5.58	0.94	17.44	0.74	1.10×10^{-4}	3.33×10^{-4}	12.05 (11.48)	PBDB-T	1.0% DIO	62
IT-DM	1.63	−3.93	−5.56	0.97	16.48	0.71	4.70×10^{-5}	2.29×10^{-4}	11.29 (10.79)	PBDB-T	1.0% DIO	62
IT-4F	1.51	−4.14	−5.66	0.88	20.88	0.71	4.32×10^{-4}	3.25×10^{-4}	13.10 (—)	PBDBT-SF	0.5% DIO	64
m-ITIC	1.58	−3.82	−5.52	0.91	18.31	0.71	1.30×10^{-4}	1.54×10^{-4}	11.77 (11.49)	J61	—	66
BT-IC	1.43	−3.85	−5.43	0.90	17.75	0.66	7.60×10^{-4}	3.53×10^{-4}	10.46 (10.28)	J71	—	67

[a] Determined by space charge limited current (SCLC) measurements using electron only devices. [b] Determined by space charge limited current (SCLC) measurements using hole only devices. [c] Average PCE values are shown in parentheses.

achieved in these devices, likely to be a result of imbalanced hole and electron mobilities in the blend ($\mu_e = 1.0 \times 10^{-4}$ cm^2 V^{-1} s^{-1} and $\mu_h = 4.5 \times 10^{-4}$ cm^2 V^{-1} s^{-1}), and domains of around 30 nm; somewhat larger than the exciton diffusion length in organic materials (Table 2). This can be attributed to the highly planar nature of the acceptor, inducing excessive crystallisation. A V_{OC} of 0.97 V was reached in these cells, which, when considering that the difference between the HOMO of the donor and the LUMO of the acceptor is only ~1.4 eV, is evidence of surprisingly low losses in this system. Despite the low FF, the devices were able to achieve a PCE of 6.3%, the highest at the time for small molecule acceptor devices. Devices using **IEIC** were later improved upon when PffT2-FTAZ-2DT was instead chosen as the donor polymer.[46] This polymer possessed a medium bandgap, allowing the active layer to achieve greater spectral coverage. Additionally, this polymer was able to form a more favourable morphology with the **IEIC** (~20 nm domains) and more balanced charge transport properties, leading to a much improved FF of 0.62. Overall, by changing the polymer to obtain a more favourable morphology and charge transport properties, an increase in PCE to 7.30% was achieved. This highlights the importance of pairing the acceptor with a polymer that is able to form favourable morphologies, as well as the correct energetics and complimentary absorption profiles. A small structural change to the structure of **IEIC** was designed where alkoxy, rather than alkyl, solubilizing groups on the thiophene spacers were employed resulting in **IEICO**.[47] Using DFT calculations (geometry optimization based on DFT at B3LYP/6-31G(d,p) level), it was found that whilst the inclusion of alkoxy chains had no effect on the HOMO and LUMO distributions, the stronger electron donating nature of alkoxy chains acted to raise the HOMO level by ~0.2 eV, thereby narrowing the bandgap of the acceptor to 1.34 eV. **IEICO** was then blended with PBDTTT-E-T to produce solar cell devices. The narrower bandgap of the acceptor led to improved spectral coverage and a broader EQE was reported, this improved photon harvesting was reflected by an improved J_{SC} of 17.7 mA cm^{-2}. A more preferable active layer morphology was also observed in comparison to their **IEIC** reference device, and diminished bimolecular recombination was observed, overall leading to the achievement of an 8.40% PCE. Another analogue of **IEIC** was reported in which the sulfur atoms in the IDT unit had been replaced by selenium atoms, producing **IDSe-T-IC**.[48] This acceptor possessed similar energy levels to **IEIC**; with a small amount of narrowing of the bandgap (1.52 eV). This is typical upon substituting thiophene for selenophene type moieties as the larger chalcogen atoms reduce the chalcogenophene's aromaticity, thereby increasing the quinoidal character of the unit and narrowing the bandgap. Possessing a slightly narrower bandgap and being blended with the donor polymer J51, which has a complimentary absorption to **IDSe-T-IC**, devices using this blend were able to achieve a J_{SC} of 15.2 mA cm^{-2}, and with similar FMOs it was able to achieve a V_{OC} of 0.91 V in devices. The morphology of the blend contained a fibrous, interpenetrating structure, which is important for efficient charge transport and reducing recombination in the blend. The presence of this morphological feature is likely to be the reason for the improved FF observed relative to **IEIC** and **IEICO** devices. As a result, **IDSe-T-IC** was able to exhibit an impressive performance of 8.58% PCE. Whilst they can lead to improved performance, selenophene containing acceptors are unlikely to be suitable candidates for commercialization due to toxicity and environmental concerns associated with them.

Open Access Article. Published on 26 April 2018. Downloaded on 3/28/2024 5:48:32 PM.
This article is licensed under a Creative Commons Attribution 3.0 Unported Licence.

O-IDTBR and **EH-IDTBR**, also made use of the IDT core; replacing the fluorene donor unit in the analogous acceptor, **FBR**.[49] The use of a more electron donating core, still flanked by BT and 3-ethylrhodanine units, resulted in a much narrower bandgap (1.63 eV). However, another important feature contributing to the reduced bandgap is the planarization that occurs when using IDT. The thienyl–phenyl link between the IDT and BT units is much less sterically strained and the single crystal X-ray structure exhibited no twist in **O-IDTBR**'s backbone, compared to the DFT calculated 34° twist in **FBR**. Again, in reducing the twisting in the molecule, the effective conjugation was increased, producing a narrowing of the bandgap, and the greater oscillator strength of the acceptor increased the absorption coefficient in **O-IDTBR** and **EH-IDTBR** compared to **FBR**. Additionally, the planarity of these acceptors also allows greater self-aggregation, which was necessary to avoid the molecular mixing that limited the performance of **FBR** devices. When **O-IDTBR** devices were fabricated with P3HT as the donor polymer, they were able to improve considerably upon the performance of **FBR**. Whilst a small drop in V_{OC} was observed (0.73 V), which can be attributed to the deeper lying LUMO, a vast improvement was seen in J_{SC}, reaching 14.4 mA cm^{-2}. This resulted in a PCE of 6.38%, which is amongst the highest for P3HT solar cells. The photocurrent was able to almost double due to the complimentary absorption of the donor and acceptor in the blend, and the formation of nanoscale acceptor domains, reduced recombination in the blend. Another notable feature of this system was the excellent oxidative stability in comparison to a number of fullerene devices, using either P3HT, PTB7-Th or PffBT4T-2DT as the donor polymer. After 1200 h in air, the low bandgap PTB7-Th:PCBM and PffBT4T-2DT:PCBM devices had dropped to less than 1% of their initial PCE, the P3HT:PCBM cell had dropped to about 10% of its initial PCE but the P3HT:O-IDTBR device retained over 73% of its initial PCE. **O-IDTBR** has also been used successfully in ternary solar cells, with P3HT as the polymer donor and **O-IDFBR** as a second electron acceptor.[50] **O-IDFBR** can be considered as analogous to **O-IDTBR**, differing in that it uses an indeno[1,2-*b*]-fluorene moiety as its electron rich core. This acceptor possesses similar phenyl–phenyl links as had been previously seen in **FBR**, affording a medium bandgap. In this system the **O-IDFBR** is used to improve upon the performance of **O-IDTBR**:P3HT binary solar cells. The inclusion of the second NFA afforded: (i) a greater V_{OC} (0.87 V), due to its higher lying LUMO; (ii) slightly improved J_{SC} (14.70 mA cm^{-2}) due to the improved spectral coverage given by using a medium and narrow bandgap acceptor; (iii) an improvement in FF (0.65), as a result of the a more favourable energy cascade in the ternary blend, and thus lower recombinative losses. Improvements in each of the V_{OC}, J_{SC} and FF led to a significant improvement in PCE, achieving a maximum of 7.80%, the highest reported efficiency for a single junction device with P3HT. The ability to produce reasonably high efficiency devices with P3HT as the donor represents an important benchmark for commercial OPV; P3HT is likely to be one of very few polymer donors that can be produced on the industrial scale currently. As such, developing high efficiency and stable devices using P3HT should be an area of focus to move closer to commercially viable OPV technologies. **EH-IDTBR** is a branched chain analogue of **O-IDTBR**, and was able to achieve a similar performance when used with P3HT.[49] Interestingly, a recent study reported that when used in combination with the low bandgap polymer PffBT4T-2DT, OPV devices were able to achieve 11.1% PCE using a non-chlorinated processing solvent, mesitylene, and without the use of additives.[51] The development of non-chlorinated device processing is important, as many chlorinated solvents are banned from use in industrial printing due to their inherent toxicity both to humans and the environment. Thus, for OPV to be viable on a large scale, alternative processing systems must be explored. By using **EH-IDTBR** with a low bandgap polymer, possessing a deeper lying HOMO than P3HT, the devices were able to achieve a V_{OC} of 1.02 V, and despite the similar absorption profile of the donor and acceptor, a J_{SC} of 17.2 mA cm^{-2}. The high photocurrent is likely to be due to excellent harvesting of photons in the 500–700 nm region of the spectrum and a favourable active layer morphology. Additionally, the devices processed from mesitylene were in fact able to exceed the efficiency achieved by chlorobenzene (CB) processed devices, the traditional solvent of choice in OPV processing, and presented better reproducibility, shelf-life and operating stability than those processed from CB.

IDT-2BR is analogous to the **IDTBR** acceptors however it contains phenylhexyl solubilizing chains on the IDT core.[52] The only optoelectronic change that the addition of the phenyl units in the solubilizing chains had caused was a slight raising of the HOMO and LUMO levels by ~0.1 eV. As such, when incorporated into devices with P3HT, a small improvement in V_{OC} to 0.84 V was observed, and an improvement in FF to 0.68 was also reported. However a drastically reduced J_{SC} of just 8.91 mA cm^{-2} was attained by the **IDT-2BR** devices, which led to an overall PCE of 5.12%. The fact that these devices were fabricated in a conventional (ITO/PEDOT:PSS/active layer/Ca/Al) architecture whereas the **O-IDTBR** devices were fabricated using an inverted (ITO/ZnO/active layer/MoO_3/Ag) architecture may account for the vast difference in J_{SC} seen between these two analogous acceptors, however the high surface roughness (15.7 nm) and a sub-optimal morphology may also have caused the drop in photocurrent in the **IDT-2BR** devices. **IDT-2BR** has also been used with PTB7-Th in OPV devices; achieving a V_{OC} of 1.02 V and a J_{SC} of 13.4 mA cm^{-2}, this blend was able to produce a PCE of 8.3%.[53] The J_{SC} was relatively modest for a low bandgap acceptor used in combination with a high performance polymer, which is likely to be a result of a sub-optimal morphology leading to significant recombination in the blend. However, the non-crystalline nature of the acceptors did lead to excellent thermal and morphological stability exhibited by the blends, something that is considered to be a major issue in fullerene containing devices. A more recent study, which also made use of PTB7-Th as the donor, compared **IDT-2BR** to **IDT-2BR1**, an analogous acceptor with *n*-hexyl solubilizing chains rather than phenylhexyl chains.[54] It was found that **IDT-2BR1** performed significantly better in devices, attaining a maximum PCE of 8.7%, in comparison to 8.3% when **IDT-2BR** was used. Again, the disparity between the two devices was mainly manifested in a much lower photocurrent when using **IDT-2BR** as the acceptor, it is suggested

 This journal is © The Royal Society of Chemistry 2019

Open Access Article. Published on 26 April 2018. Downloaded on 3/28/2024 5:48:32 PM.
This article is licensed under a Creative Commons Attribution 3.0 Unported Licence.

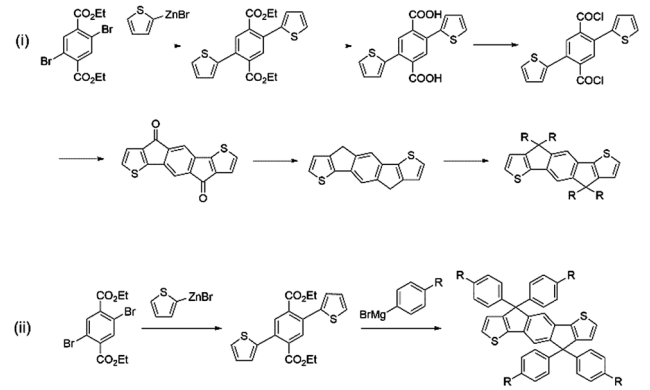

Fig. 6 Synthetic procedures for the preparation of IDT with (i) aliphatic alkyl chains and (ii) aromatic alkyl chains at the carbon bridgehead positions.

that this is a result of the *n*-hexyl chains of **IDT-2BR1**, which allowed stronger 3D intermolecular interactions with the donor material and greater electron mobilities (μ_e = 3.9 × 10^{-4} cm^2 V^{-1} s^{-1} and μ_h = 1.5 × 10^{-4} cm^2 V^{-1} s^{-1} for the **IDT-2BR1** blend *cf.* μ_e = 1.7 × 10^{-4} cm^2 V^{-1} s^{-1} and μ_h = 6.7 × 10^{-4} cm^2 V^{-1} s^{-1} for the **IDT-2BR** blend). Therefore, despite a slightly more simple synthetic route available for **IDT-2BR** and other IDT based acceptors that make use of arylalkyl rather than alkyl side chains, this study seems to suggest that the inclusion of the phenyl units on the solubilizing chains lead to inferior intermolecular interactions, a less favourable morphology and thus poorer performance in devices. The widespread use of the IDT moiety in A–D–A type acceptors means that any distinction in performance between alkyl and aryl–alkyl IDT should be further investigated; allowing focus to shift to the more suitable IDT analogue (Fig. 6).

The design of **IDT-2BR** was further extended by substituting the electron withdrawing BT spacer unit with thieno[3,4-*b*]thiophene (TT) and dicyanovinyl moieties were included on the rhodanine units, in the acceptor **ATT-1**.[55] This acceptor exhibited a reduced bandgap (1.54 eV) due to the inclusion of the strongly electron withdrawing dicyanovinyl rhodanine and a small increase in planarity, arising from the inclusion of the TT unit. When OPV devices were made, using PTB7-Th as the donor, an improved PCE of 10.07% was reported, relative to the 8.30% with **IDT-2BR**. The narrowing of the bandgap of **ATT-1** arose from a lower lying LUMO, and therefore a decrease in V_{OC} to 0.87 V, however the narrower bandgap and stronger extinction coefficient of this acceptor led to improved photon harvesting, when compared to **IDT-2BR**, and thus a substantial increase in J_{SC} to 16.48 mA cm^{-2}. It was necessary to use DIO in order to achieve this high efficiency, by enhancing the acceptor crystallinity and reducing the tendency for the donor and acceptor to mix. Though this led to a substantially improved performance, systems that require the use of additives such as DIO are not particularly attractive from an industrial viewpoint, as a result of the photostability problems that they have been noted to cause.

ITIC can be considered as a further development of the acceptor **IEIC**, this acceptor made use of IDTT as the core, rather than IDT, and did not include a π-conjugated spacer, with the electron deficient DCI units on the periphery.[56] The extension of the electron donating core and removal of the π-conjugated spacer in **ITIC** produced a very similar bandgap (1.59 eV) to that exhibited by **IEIC** (Fig. 7). However, the HOMO and LUMO values were shifted upwards by ~0.1 eV. When paired with PTB7-Th, the OPV devices exhibited a V_{OC} of 0.81 V; this is slightly lower than seen for **IEIC**, which may be a result of increased energetic losses in this system. The devices showed a similarly high J_{SC} of 14.22 mA cm^{-2}, but the most marked improvement was in FF (0.59) due to more closely balanced hole and electron mobilities in the blend (μ_e = 1.1 × 10^{-4} cm^2 V^{-1} s^{-1} and μ_h = 4.3 × 10^{-5} cm^2 V^{-1} s^{-1} for the **ITIC** blend *cf.* μ_e = 1.0 × 10^{-4} cm^2 V^{-1} s^{-1} and μ_h = 4.5 × 10^{-4} cm^2 V^{-1} s^{-1} for the **IEIC** blend), thereby reducing recombination. This resulted in a maximum PCE of 6.8% being achieved. There have since been several improvements made using this acceptor with medium and wide bandgap polymer donors. However, the most notable of these is the recent report where **ITIC** was paired with a wide bandgap polymer PBQ-4F to produce devices that were able to achieve 11.34% PCE.[57] An improvement in J_{SC} was observed arising from the improved photon harvesting that is possible with the complimentary

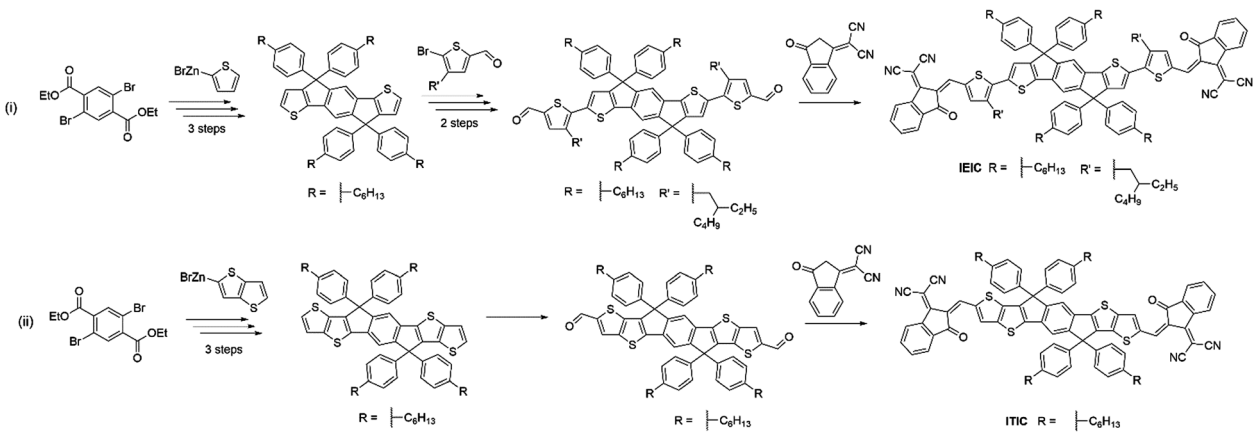

Fig. 7 Comparison of the synthetic routes required for (i) IDT based **IEIC** and (ii) IDTT based **ITIC**.

Open Access Article. Published on 26 April 2018. Downloaded on 3/28/2024 5:48:32 PM.
This article is licensed under a Creative Commons Attribution 3.0 Unported Licence.

absorption of the polymer and acceptor. A vastly improved FF (0.67) can be considered as a result of much higher hole and electron mobilities, that were also more closely balanced (μ_e = 1.0 × 10^{-3} cm^2 V^{-1} s^{-1} and μ_h = 1.0 × 10^{-3} cm^2 V^{-1} s^{-1}), leading to reduced recombinative losses in the blend. Strong π–π interactions between the donor polymer, likely a result of PBQ-4F's planar structure, improved the charge transport properties of the blend. Importantly, the active layers of the high efficiency devices reported here are also processed from a relatively benign non-chlorinated solvent system, tetrahydrofuran (THF) with 5% isopropanol as an additive. As highlighted above for the PffBT4T-2DT:EH-IDTBR solar cells that were also processed from non-chlorinated solvents, this is an important step towards realising commercially viable OPV. **ITIC-Th** is an analogue of **ITIC** in which the phenyl units of the solubilizing sidechains have been replaced by thienyl groups.[58] Relative to its phenyl containing counterpart, **ITIC-Th** possesses slightly deeper lying HOMO and LUMO levels; a result of the electron withdrawing σ-inductive effect from the thienyl moieties. Additionally, the inclusion of the thienyl–alkyl chains led to enhanced intermolecular interactions, and therefore an improved electron mobility for **ITIC-Th** (μ_e = 6.1 × 10^{-4} cm^2 V^{-1} s^{-1} for the **ITIC-Th** blend *cf.* μ_e = 2.6 × 10^{-4} cm^2 V^{-1} s^{-1} for the **ITIC** blend). In devices with PDBT-T1, this acceptor was able to reach 9.6% PCE, with a high J_{SC} of 16.24 mA cm^{-2} resulting from the complimentary absorption and preferred morphology in the bulk heterojunction. The outstanding feature of this acceptor is a high FF of 0.67 being achieved, mainly as a product of the high and balanced charge carrier mobilities exhibited by this blend. However, it must be noted that to achieve the optimal morphology, 1-chloronaphthalene (CN), a chlorinated high boiling point additive was needed. Whilst this can improve the performance in OPV devices, if they persist in the active layer they can significantly lower the morphological stability of the blends over time, leading to microscale phase separation.[59] Building upon this promising result, **ITIC-Th** was combined with a less crystalline, medium bandgap donor polymer, PTFB-O.[60] This allowed the formations of much smaller domains in the bulk heterojunction (~30 nm) and high PL quenching was observed, suggesting that the excitons can be split into free charges more efficiently and non-geminate recombinative losses can be minimized. This led to the impressive photocurrent and fill factor (17.6 mA cm^{-2} and 0.69) and ultimately a PCE of 10.88% without the use of any additives.

IC-C6IDT-IC makes use of an alkylated IDT core, in this case with *n*-hexyl chains rather than the phenyl or thienyl alkyl chains. Again, use is made of the DCI end group, without the use of a π-conjugated spacer in the molecule.[61] This afforded a bandgap of 1.62 eV despite its structural simplicity, relative to the aforementioned IDT and IDTT based acceptors, and possessed HOMO and LUMO levels similar to the **IDTBR** acceptors. **IC-C6IDT-IC** was paired with a medium bandgap donor polymer in devices (PDBT-T1) and was among the first examples of A–D–A type NFA solar cells to reach a PCE of over 8%, in this case reaching 8.71%. Through the complimentary absorption profiles of the donor and acceptor, along with the strong absorption coefficient, this blend was able to reach photocurrents of 15.05 mA cm^{-2}. Preferential face-on π–π ordering and appropriate length scale phase separation was suggested to lead to relatively good charge carrier mobilities in the blend (μ_e = 2.9 × 10^{-4} cm^2 V^{-1} s^{-1} and μ_h = 5.1 × 10^{-5} cm^2 V^{-1} s^{-1}), further contributing to the high J_{SC} and FF (0.67) exhibited by this blend.

A further development in the design of **ITIC** based acceptors by introducing either one or two methyl groups onto the phenyl ring of the DCI unit, to create **IT-M** and **IT-DM**.[62] The aim of these modifications was to raise the LUMO slightly, in order to improve the V_{OC}, without causing additional morphological disruption, hence very short methyl units were used. The inclusion of the weakly electron donating methyl groups had the desired effect, with **IT-M** possessing a LUMO which was 0.04 eV higher than their value measured for **ITIC**, and **IT-DM** possessing a LUMO that was 0.09 eV higher. The acceptors were paired with the donor polymer PBDB-T, which had already shown reasonable success with **ITIC**; achieving 11.2%.[63] **IT-M** was able to achieve an improved V_{OC} of 0.94 V (relative to the 0.90 V achieved in PBDB-T:ITIC devices) as a result of the higher lying LUMO, but also had an superior J_{SC} which was ~1 mA cm^{-2} higher (17.44 mA cm^{-2}) than the **ITIC** reference device. The result of which was a PCE of 12.05%, among the highest currently reported fullerene-free single-junction OPVs. **IT-DM** was able to further improve on the V_{OC} to 0.97 V, however the J_{SC} and FF dropped slightly, leading to a still impressive 11.29% PCE. The poorer J_{SC} and FF in devices containing **IT-DM** were attributed to a slight reduction in domain purity, which led to a small increase in exciton dissociation efficiency and asymmetric charge transport properties. A similar strategy has since been employed in the design of **IT-4F**.[64] In this case the phenyl units of the DCI end group each contain 2 fluorine atoms, rather than the methyl groups used in **IT-M** and **IT-DM**. The inclusion of the fluorine atoms was aimed to narrow the bandgap further, and improve both intra- and intermolecular interactions through the non-covalent F···H and S···F interactions that can often be observed in fluorinated molecules.[65] As expected the fluorination of the DCI end group led to a lowering of both the HOMO and LUMO levels due to the strong electron withdrawing nature of the fluorine atoms. Stronger π–π interactions led to a broadened and red shifted absorption spectrum, along with an enhanced extinction coefficient due to enhanced intramolecular charge transfer, in **IT-4F**. The improved intermolecular interactions also led to a slight gain in the electron mobility of the acceptor (μ_e = 4.32 × 10^{-4} cm^2 V^{-1} s^{-1} for the **IT-4F** blend *cf.* 3.13 × 10^{-4} cm^2 V^{-1} s^{-1} for the **ITIC** blend). As a result of the lowered FMOs of **IT-4F**, PBDB-T was no longer the optimal candidate to be used in bulk heterojunctions as the offset between the HOMO of the donor and the LUMO of the acceptor would not have been able to produce a respectable V_{OC} in devices. Instead a modified version of the polymer (PBDB-T-SF) was developed, which was fluorinated on the thienyl units of the side-chains. This again led to a lowering of the FMOs and similar improvements in the optical and charge carrier transport properties. OPV devices utilizing **IT-4F** and PBDB-T-SF were able to achieve an exceptional 13.1% PCE, the highest reported in single-junction polymer solar cells to date. Despite having a lower

 This journal is © The Royal Society of Chemistry 2019

Open Access Article. Published on 26 April 2018. Downloaded on 3/28/2024 5:48:32 PM.
This article is licensed under a Creative Commons Attribution 3.0 Unported Licence.

V_{OC} than devices using most **ITIC** based acceptors (0.88 V), a vast improvement in J_{SC} to 20.88 mA cm^{-2} was apparent as a result of the enhanced photon harvesting made possible by the more strongly absorbing components. It must be recognized that the chemical modification of the polymer also contributed to the improved performance, highlighting the benefit of tuning the donor polymer to better suit the acceptor. These devices were also shown to display excellent storage stability under N_2, still achieving 11.99% after 1700 h. **m-ITIC**, another derivative of **ITIC** has also been reported in which the position of the solubilizing alkyl substituent has been moved from the *para*- to the *meta*-position on the phenyl rings.[66] The design strategy behind this side-chain isomerization was to tune the intermolecular self-assembly of the acceptor without altering the optoelectronic properties of the acceptor substantially. The FMOs remained very similar to those of **ITIC**, and no obvious changes in the optical properties were reported. The isomerization of the side-chain did however have a significant impact on the crystallinity of the acceptor, whereby the *para*-alkyl–phenyl version (**ITIC**) had poorer self-organization than the *meta*-alkyl–phenyl **m-ITIC**; this was apparent from better defined scattering peaks in GIWAXS and a longer crystalline correlation length (CCL). Additionally, **m-ITIC** adopted a predominantly face-on crystalline orientation in these devices, compared to the co-existence of both edge-on and face-on crystallites in **ITIC** devices. The more crystalline nature and preferential face-on orientation of crystallites in **m-ITIC** gave rise to a greater electron mobility (μ_e = 1.30 × 10^{-4} cm^2 V^{-1} s^{-1} for the **m-ITIC** blend *cf.* μ_e = 1.05 × 10^{-4} cm^2 V^{-1} s^{-1} for the **ITIC** blend). The acceptor was blended with a medium bandgap donor polymer J61, with reference devices using **ITIC** also fabricated. The virtually identical FMOs of the two acceptors led to a very similar V_{OC} in both cases (0.91 V), however the improved electron mobility of **m-ITIC** led to a more balanced charge transport in the blend, resulting in reduced recombination in the bulk heterojunction. This was reflected in a large increase in FF for the **m-ITIC** devices relative to the reference **ITIC** devices; 0.71 and 0.66 respectively. This led to an overall improvement in PCE from 10.57% to 10.77% upon modifying the acceptor to contain the *meta*-phenyl–alkyl chains. Therefore, in addition to the consideration of alkyl *vs.* aryl–alkyl chains on the acceptor, isomerization of the aryl–alkyl chains can also play a role in fine tuning the structural and morphological properties of NFAs.

BT-IC, an extremely low bandgap acceptor, comprised of a BDT core unit, which was fused with cyclopentadithiophene units on either side to produce a fused seven ring system, flanked by the electron deficient DCI end groups.[67] This acceptor included electron donating alkoxy chains on the BDT part of the fused ring core to raise the HOMO, and narrow the bandgap further without lowering the LUMO, thus avoiding the possibility of a lower V_{OC}. The added electron-donating nature of this core unit allowed a remarkably low bandgap of 1.43 eV to be achieved, and still retained an extinction coefficient that was comparable to **ITIC**. This allowed greater spectral coverage when blended with J71, a medium bandgap donor polymer, resulting in a respectable J_{SC} of 17.75 mA cm^{-2}. The strategy of including alkoxy chains to raise the HOMO and narrow the bandgap, without impacting the LUMO, also proved to be successful with a V_{OC} of 0.90 V being achieved. Overall this resulted in a PCE of 10.46%, however the increased synthetic complexity relative to **ITIC** is not offset by any outstanding improvements in performance.

There are several key points that can be taken away from the evolution of the A–D–A type acceptors discussed above. The early fluorene based acceptors showed considerable promise, but ultimately the push–pull character and conjugation afforded in many of these materials was not sufficient to harvest many of the high-energy photons effectively. Additionally, the inherent twisting in a number of these acceptors, caused by the steric clash of ortho-hydrogen atoms in the phenyl–phenyl linkages, led to poorly aggregating materials that mixed too finely with the donor polymer in active layer blends. The IDT based acceptors that evolved from the above issues have led to significant progress. Increased conjugation and push–pull character has allowed narrow bandgaps to be accessed in NFAs, and therefore improved photon absorption. While, the extended planar structures achieved a greater tendency for aggregation of the acceptors in blends, often leading to favourable length-scale percolating networks of donor and acceptor materials in the blends. The relative aggregation tendency of the acceptor, necessary for optimal device performance, depends heavily on the crystallinity of the donor polymer used. However, a general rule is apparent that if the acceptor does not exhibit a strong tendency to aggregate and phase separate it will molecularly mix with the polymer, resulting in large recombinative losses and reduced electron mobility. Alternatively, acceptors with a high aggregation tendency will often form domains that are far larger than the exciton diffusion length, leading to a larger fraction of excitons relaxing before reaching the interface and are therefore wasted. Hence, a balance between these two extremes must be reached in order to achieve donor and acceptor domains that are on the same lengthscale as the exciton diffusion length, leading to an optimal blend morphology. As the successful A–D–A structures have become more apparent, diligent work to tune the solubilizing chains, located both on the core and the end groups, has led to a fine-tuning of the aggregation properties of the acceptors and consequently improved bulk-heterojunction morphologies and device performance. Though this has allowed incremental improvements in PCE, care must be taken not to compromise the synthetic complexity of these acceptors in the pursuit of higher efficiencies such that they are not viable to produce on an industrial scale. Further to this, the inclusion of a handful of studies reporting OPV devices fabricated from non-chlorinated solvents whilst using A–D–A type NFAs highlights another advantage this class of acceptors holds, in addition to the highest efficiencies currently reported. With >11% PCE now achieved on a routine basis, it may allow a shift of focus to improve the stability of materials in devices and lowering the costs associated with the preparation of these acceptors. Another important consideration is to design NFAs that are compatible with scalable donor polymers. Though the most exceptional efficiencies have been achieved with low bandgap polymers, P3HT remains to be the only truly scalable donor to date. Therefore, further optimization of the A–D–A type acceptors

Open Access Article. Published on 26 April 2018. Downloaded on 3/28/2024 5:48:32 PM.
This article is licensed under a Creative Commons Attribution 3.0 Unported Licence.

should have some focus, at least, on improving upon the best P3HT:NFA systems that have been reported.

3. Perylene diimide based acceptors

Perylene-3,4:9,10-tetracarboxylic acid diimides (PDIs) are a class of π-conjugated molecules that over the past three decades have found extensive applications as high-performance organic semiconductors, and have found relative success in the field of organic photovoltaics. Whilst their electron-withdrawing character arises from their dicarboxylic acid imide groups at the 3,4- and 9,10-*peri*-positions, their polycyclic aromatic skeleton acts as electron-donating unit. The optoelectronic properties of this class of NFAs can further be influenced through the inclusion of alkyl, aryl or heteroaryl substituents at their core (1,2,5,6,7,8,11,12) positions. Since the imide nitrogen is not conjugated to the aromatic system, functional group substitution at these positions does not tend to affect the FMOs and is instead used to tune the self-assembly properties of these acceptors, thus allowing for a partially independent modulation of the opto-electronic and morphological properties. Compared to A–D–A type acceptors, the vast aromatic system of PDIs is highly beneficial to their charge carrier mobilities with electron mobilities over 1 $cm^2 V^{-1} s^{-1}$ having been reported.[68] Moreover, their good electron accepting properties and excellent thermal, chemical and photochemical stability add to their attractiveness.[69,70] The main drawback of PDIs as NFAs is their extended π-scaffold often leading to micrometer-sized aggregates in blends, which in turn leads to insufficiently large donor–acceptor interfaces for efficient exciton splitting. Consequently, over the past 30 years numerous molecular engineering strategies have been dedicated towards striking a balance between the formation of donor-PDI domains that are sufficiently small to allow for efficient charge separation, yet large enough to ensure percolating networks for high charge carrier mobilities.[71] Three main approaches have been developed towards optimising PDI's optoelectronic and morphological properties in OPV blends, these rely on chemical modifications at either the imide, bay (1,6,7,12) or *ortho* (2,5,8,11) positions of the PDI core (Fig. 8).

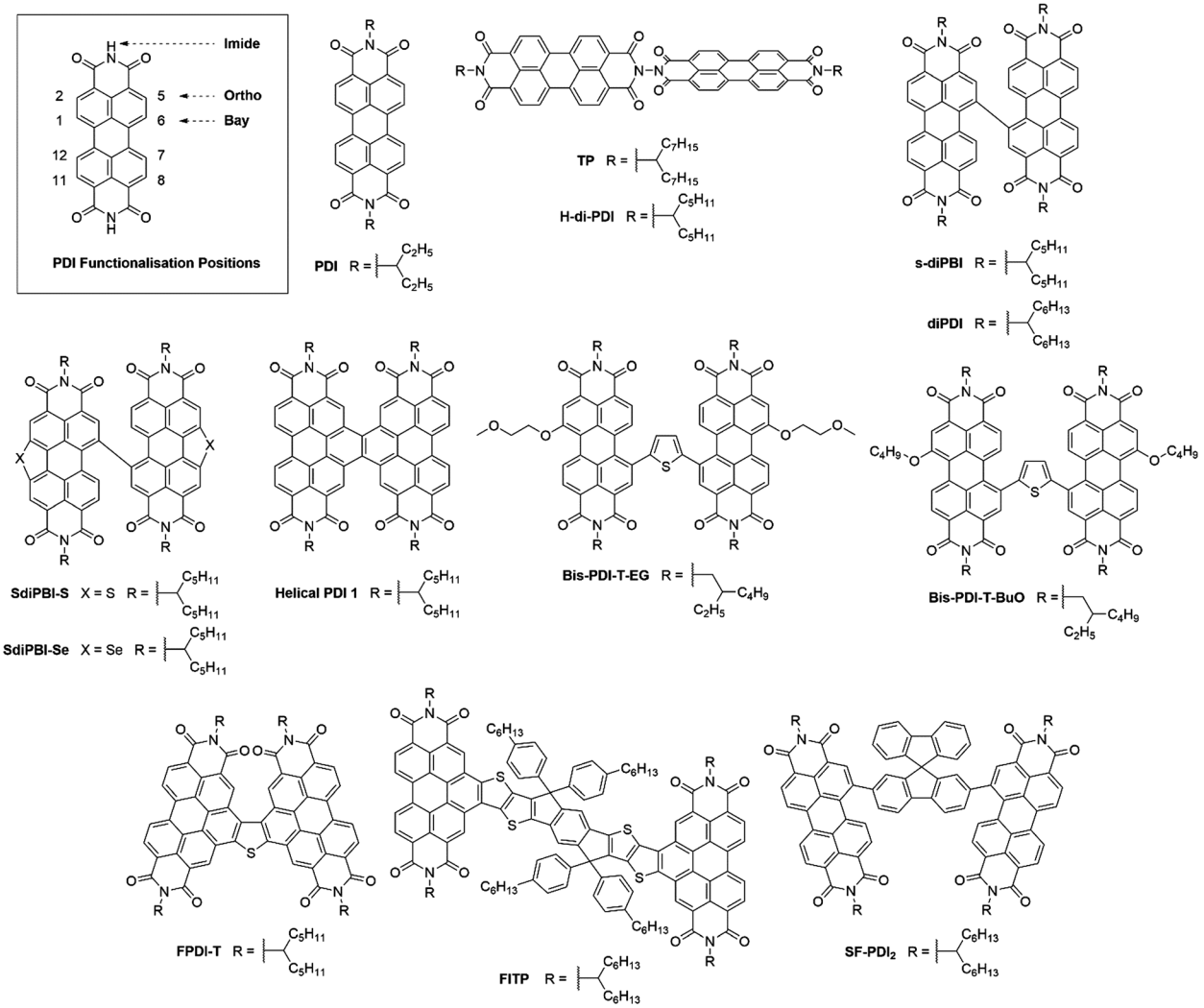

Fig. 8 Monomeric and dimeric PDI based small molecule acceptors.

Open Access Article. Published on 26 April 2018. Downloaded on 3/28/2024 5:48:32 PM.
This article is licensed under a Creative Commons Attribution 3.0 Unported Licence.

3.1. PDI monomers

The oldest and simplest strategy to control the aggregation tendency of PDIs involves the inclusion of solubilising side chains. A well-known and highly studied example thereof is **PDI**, bearing pendant 1-ethyl-propyl chains at either imide nitrogen atom. Although initial investigations of **PDI** as a NFA only yielded devices with PCEs <1%, successful fabrication of devices with a PCE of 3.0% was achieved, when blending **PDI** with the low bandgap small molecule donor *p*-DTS(FBTTh$_2$)$_2$ (Table 3).[72,73] The increase in the photocurrent (7.4 mA cm^{-2}) was attributed to the complementary absorption of the donor and the acceptor leading to greater spectral coverage compared to the previously reported active layer blends. Further incrementation of the performance of *p*-DTS(FBTTh$_2$)$_2$:**PDI** based devices was achieved by optimising the donor:acceptor ratio from 1 : 1 to 1.3 : 1. Due to *p*-DTS(FBTTh$_2$)$_2$'s greater molar extinction coefficient compared to **PDI**, increasing the donor percentage in the blend allowed for 10% more intense light absorption compared to the 1 : 1 reference blend.[74] Additionally, transmission electron microscopy (TEM) revealed smaller phase domains, around 20 nm, in the 1.3 : 1 blends that should allow for more efficient exciton splitting. Photoluminescence quenching measurements confirmed the more suitable blend morphology as the fluorescence from the donor and the acceptor were minimised at the higher donor concentration in the blend. Better charge generation by tuning of the optical and morphological properties of the blend thus rationalise the 35% improved photocurrent in devices with a maximum PCE of 5.13%.

3.2. PDI dimers

An alternative strategy to disrupt PDIs' cofacial stacking involves the use of dimeric PDI acceptors with twisted conformations. **TP** was conveniently synthesised in a four-step route with an overall yield of 34%, whereby the two PDI units are connected by a hydrazine linkage and rotated orthogonally to each other.[75] The use of a highly twisted 3D structure was intended to inhibit the excessive aggregation often observed in PDI containing blends, leading to a percolating donor:acceptor network on the correct length scale, rather than the unfavourable formation of micrometer sized domains observed in active layers where aggregation has not been suppressed. When used in combination with the low bandgap polymer donor PBDTTT-C-T, this acceptor was able to achieve a PCE of 3.20%. The good photovoltaic performance was attributed to the optimum domain sizes around 10 nm in the active layer allowing for efficient charge generation and transport. **TP**'s design concept was then developed further with the acceptor **H-di-PDI**. Again, this acceptor utilised a hydrazine linked PDI dimer, but employed pentyl–hexyl rather than heptyl–octyl solubilising chains.[76] Shortened side-chains allowed for tighter molecular packing, such that higher charge carrier mobilities could be achieved (μ_e = 4.3 × 10^{-4} cm^2 V^{-1} s^{-1} and μ_h = 2.3 × 10^{-2} cm^2 V^{-1} s^{-1} for the **H-di-PDI** blend *cf.* μ_e = 1.47 × 10^{-4} cm^2 V^{-1} s^{-1} and μ_h = 2.74 × 10^{-4} cm^2 V^{-1} s^{-1} for the **TP** blend). Using PTB7-Th as the donor material, devices were able to achieve a much improved PCE of 6.41%. Whilst PTB7-Th's lower bandgap allowed for greater spectral coverage hence photocurrents, the higher charge carrier mobilities ensured a 30% larger fill factor (Fig. 9).

Table 3 Summary of the optoelectronic properties of monomeric and dimeric PDI based small molecule acceptors and their *J*–*V* characteristics in bulk heterojunction solar cells

Acceptor	Optical E_g (eV)	HOMO (eV)	LUMO (eV)	V_{OC} (V)	J_{SC} (mA cm^{-2})	FF	Electron mobility[a] (cm^2 V^{-1} s^{-1})	Hole mobility[b] (cm^2 V^{-1} s^{-1})	PCE[c] (%)	Donor	Additive	Ref.
PDI	—	—	—	0.78	7.4	0.52	1.70 × 10^{-4}	7.40 × 10^{-5}	3.00 (—)	*p*-DTS(FBTTh$_2$)$_2$	0.4% DIO	73
PDI	—	−5.87	−3.82	0.8	10.1	0.64	4.50 × 10^{-3}	1.61	5.13 (5.07)	*p*-DTS(FBTTh$_2$)$_2$	0.4% DIO	74
TP	—	—	—	0.77	9.0	0.46	1.47 × 10^{-4}	2.74 × 10^{-4}	3.20 (—)	PBDTTT-C-T	—	75
H-di-PDI	2.09	−5.85	−3.74	0.79	13.1	0.60	4.30 × 10^{-4}	2.30 × 10^{-2}	6.41 (6.19)	PTB7-Th	1.0% DIO and 2.0% CN	76
s-diPBI	2.10	−5.94	−3.84	0.73	10.6	0.47	—	—	3.63 (—)	PBDTTT-C-T	1.5% DIO and 1.5% CN	77
s-diPBI	2.08	−5.95	−3.87	0.87	8.3	0.61	—	1.00 × 10^{-3}	4.39 (—)	PBDB-T	1.5% DIO and 1.5% CN	78
s-diPBI	2.09	−6.13	−4.04	0.80	12.0	0.59	3.32 × 10^{-5}	4.36 × 10^{-2}	5.90 (5.73)	PTB7-Th	1.0% DIO and 2.0% CN	79
SdiPBI-S	2.20	−6.05	−3.85	0.90	12.0	0.66	2.80 × 10^{-3}	1.20 × 10^{-3}	7.16 (6.90)	PDBT-T1	0.75% DIO	80
SdiPBI-Se	2.22	−6.09	−3.87	0.91	12.8	0.70	4.80 × 10^{-3}	3.60 × 10^{-3}	8.47 (8.23)	PDBT-T1	0.25% DIO	81
Helical PDI 1	—	—	—	0.80	13.5	0.55	3.40 × 10^{-4}	2.90 × 10^{-4}	6.05 (5.94)	PTB7-Th	1.0% DIO and 1.0% CN	82
Bis-PDI-T-EG	1.81	−5.65	−3.84	0.85	8.9	0.54	1.00 × 10^{-3}	3.00 × 10^{-3}	4.03 (3.91)	PBDTTT-C-T	5.0% DIO	83
Bis-PDI-T-EG	1.81	−5.65	−3.84	0.84	12.8	0.56	6.06 × 10^{-3}	1.03 × 10^{-2}	6.10 (6.00)	PBDTTT-C-T	1.5% DIO	84
Bis-PDI-T-EG	1.80	−5.64	−3.84	0.89	13.2	0.59	1.87 × 10^{-4}	1.63 × 10^{-4}	7.24 (6.94)	PDBT-T1	3.0% DIO	85
Bis-PDI-T-BuO	1.79	−5.65	−3.86	0.89	12.3	0.58	2.30 × 10^{-5}	4.10 × 10^{-4}	6.36 (6.18)	PDBT-T1	2.0% DIO	86
FPDI-T	2.22	−5.98	−3.77	0.93	12.0	0.58	1.63 × 10^{-4}	5.92 × 10^{-2}	6.72 (6.48)	PTB7-Th	2.0% CN	87
FITP	1.73	−5.28	−3.75	0.99	13.2	0.56	3.66 × 10^{-4}	5.60 × 10^{-4}	7.33 (—)	PTB7-Th	2.0% CN	88
SF-PDI$_2$	2.07	−5.90	−3.83	0.98	10.7	0.57	1.80 × 10^{-4}	2.30 × 10^{-3}	6.30 (6.00)	PffBT4T-2DT	—	89
SF-PDI$_2$	2.37	−5.99	−3.62	1.11	13.3	0.64	—	—	9.50 (—)	P3TEA	2.5% ODT	90

[a] Determined by space charge limited current (SCLC) measurements using electron only devices. [b] Determined by space charge limited current (SCLC) measurements using hole only devices. [c] Average PCE values are shown in parentheses.

Open Access Article. Published on 26 April 2018. Downloaded on 3/28/2024 5:48:32 PM.
This article is licensed under a Creative Commons Attribution 3.0 Unported Licence.

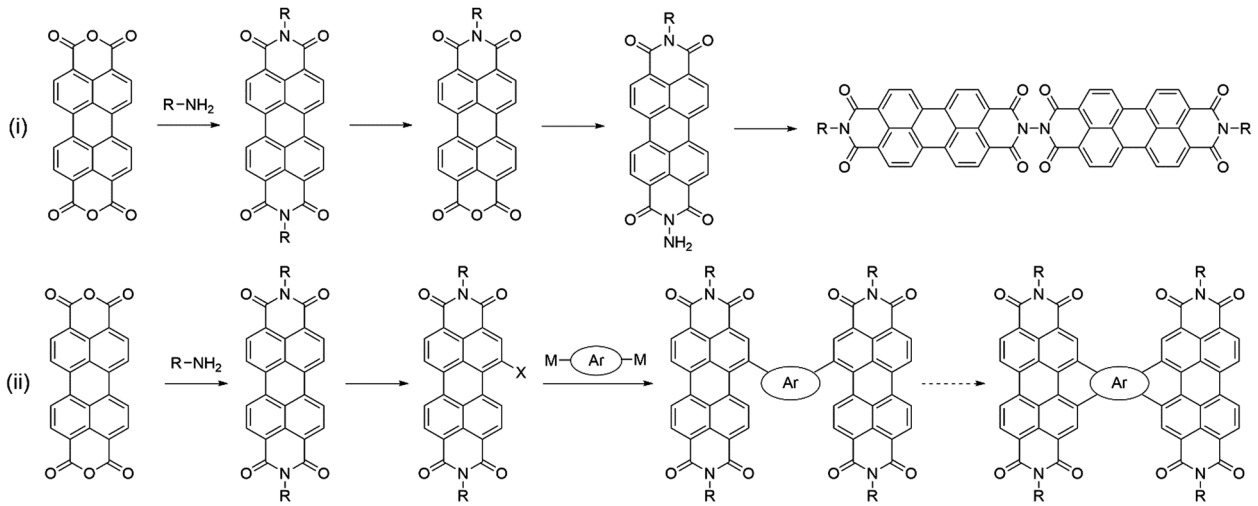

Fig. 9 Comparison of the general synthetic routes required for (i) imide linked and (ii) bay linked PDI dimers.

Twisted conformations in PDI dimers can also arise *via* linkage of the two monomers at their bay positions. Amongst the simplest and highest performing bay-linked PDI dimers is **s-diPBI**, in which the two PDI units are covalently bound through a C–C single bond at their 1-position. The 70° dihedral angle (estimated by geometry optimization using DFT with B3LYP/6-31G(d) basis sets) across the two PDI planes gives rise to the three-dimensionality of the NFA and is designed to improve the photovoltaic performance by reducing the acceptor's inherent aggregation tendency. Another important feature of the large twist angle is the resulting break in conjugation thus conferring the acceptor a relatively high lying LUMO (approx. −3.8 eV) to aid in maximising the V_{OC}. The first devices employing **s-diPBI** as NFA were fabricated by spin-coating the active layer from a PBDTTT-C-T:**s-diPBI** blend, affording cells with a PCE of 3.63%.[77] It was found that despite the acceptors high-lying LUMO, the performance was limited predominantly by poorly matched energy levels between the polymer donor and the acceptor thereby limiting the V_{OC} of the cells. Based on this observation, PDBTTT-C-T was replaced with PBDTBDD, whose deeper HOMO yielded an almost 20% larger V_{OC} thus boosting performance to 4.39%.[78] Further enhancement of the efficiency of **s-diPBI** based solar cells was achieved by switching from a conventional to an inverted device architecture.[79] In the inverted device, more intense light absorption due to reduced thin-film interference arising from more carefully managed refractive index differences led to better optical distribution. Furthermore, deposition of a $PC_{61}BM$-SAM on the ZnO ETL led to reduced charge recombination at the active layer-ZnO interface, as suggested by the increased shunt resistance and decreased reverse saturation current density. Both of these factors were responsible for an almost 50% incremental increase in the J_{SC} compared to the conventional reference, which in turn also explained the improved PCE of 5.90%. Based on **s-diPBI**'s molecular scaffold, **SdiPBI-S** was developed in a 5-step synthesis.[80] Again, the core of the NFA consisted of two bay-linked PDI monomers, yet this time the external bay positions were annulated with sulfur atoms. Heteroannulation in the bay regions was achieved by Stille coupling of **SdiPBI-S**'s tetrachloro precursor with bis(tributyltin)sulfide and was employed to induce a more twisted conformation in the acceptor, thereby raising its LUMO energy and consequentially also the V_{OC} in devices. Moreover, a more pronounced 3D character should also inhibit microscale aggregation in the active layer leading to more suitably tuned phase domains. In conventional architecture devices PDBT-T1:**SdiPBI-S** blends reached a noteworthy PCE of 7.16%. Albeit using different donors and device architectures, the increased performance of **SdiPBI-S** compared to **s-diPBI** was attributed to the increased torsional angle between the two PDI planes in **SdiPBI-S**, which reduces the conjugation between the two PDI monomers. Consequently, the acceptor's LUMO was raised, thereby contributing to the increased V_{OC} in devices. Another ramification of **SdiPBI-S**'s higher lying LUMO was a hypsochromically shifted absorption band leading to greater donor:acceptor spectral complementarity and ultimately a higher J_{SC}, reaching 11.98 mA cm^{-2}. Inspired by the successes of this molecular engineering strategy and in the pursuit of higher PCEs, the selenophene analogue of **SdiPBI-S**, **SdiPBI-Se** was synthesised.[81] It was envisaged that selenium's more diffuse and polarisable electron cloud would improve orbital overlap and intermolecular interactions thus increase the charge carrier mobility in the acceptor. GIWAXS and space-charge limited current measurements confirmed the above hypothesis by revealing shorter lamellar stacking distances and more equilibrated electron and hole mobilities in the PDBT-T1:**SdiPBI-Se** blend compared to the **SdiPBI-S** reference (μ_e = 4.8 × 10^{-3} cm^2 V^{-1} s^{-1} and μ_h = 3.6 × 10^{-3} cm^2 V^{-1} s^{-1} for the **SdiPBI-Se** blend *cf.* μ_e = 2.8 × 10^{-3} cm^2 V^{-1} s^{-1} and μ_h = 1.2 × 10^{-3} cm^2 V^{-1} s^{-1} for the **SdiPBI-S** blend). This also rationalises the then unprecedented FF of 0.70 and impressive PCE of 8.42% obtained in champion devices.

More complex bay-linked PDI structures with vinyl or aromatic bridging moieties have also shown significant potential as substitutes for fullerenes in OPVs. The general synthesis of such bay-substituted PDI dimers follows a three-step route involving

Open Access Article. Published on 26 April 2018. Downloaded on 3/28/2024 5:48:32 PM.
This article is licensed under a Creative Commons Attribution 3.0 Unported Licence.

imidisation of the commercially available perylene-3,4,9,10-tetracarboxylic dianhydride, followed by mono-bromination at the 1-position using elemental bromine and finally a palladium catalysed cross-coupling reaction to join the three fragments. Amongst the structurally simplest derivatives of this class is **Helical PDI 1**, whose PDI subunits are linked at their bay positions *via* a two-carbon bridge giving rise to a fully conjugated aromatic system.[82] The aim of this modification was to generate a highly delocalised π-system to confer intense photon absorption. The steric clashes between the C–H bonds at the internal *ortho* positions on the other hand give rise to the helical 3D structure of the NFA. In a blend with PTB7-Th, a maximum PCE of 6.05% was recorded. The high efficiency of **Helical PDI 1**'s was rationalised by femtosecond transient absorption spectroscopy (TAS), which indicated exciton photogeneration in both the donor and the acceptor domains. It was speculated that device performance could potentially be further incremented by minimising the number and extent of recombination mechanisms in the cells. Three dimensionality in PDIs can also arise through the use of heteroaromatic π-bridges. A thienyl linked PDI dimer, **Bis-PDI-T-EG** was reported where the use of a more electron donating bridging unit in the acceptor was intended to generate a push–pull structure similar to the one in calamitic shaped small molecule NFAs, which in turn should enhance both the optical transition intensity and width.[83] Cells were spin-coated from a PBDTTT-C-T:**Bis-PDI-T-EG** blend and gave a maximum PCE of 4.03%. The narrowed bandgap of the acceptor led to ameliorated spectral coverage and a broader EQE was reported, this improved photon harvesting was reflected by a J_{SC} of 8.86 mA cm^{-2}. On the other hand, atomic force microscopy (AFM) showed that a potentially limiting factor in the photocurrent, and therefore photovoltaic performance, was the unsuitably large phase domains in the active layer. In fact, in a later publication further raising of the efficiency of the **Bis-PDI-T-EG** acceptor was possible by fine tuning the film-forming kinetics of the active layer.[84] TEM revealed that judicious regulation of the solvent additive content and the solvent vapour annealing process resulted in larger fibril sizes in the active layer, thereby favouring the charge carrier mobilities and fill factor (μ_e = 6.06 × 10^{-3} cm^2 V^{-1} s^{-1} and μ_h = 1.03 × 10^{-2} cm^2 V^{-1} s^{-1} for the fibrillar **Bis-PDI-T-EG** blend *cf.* μ_e = 1.0 × 10^{-3} cm^2 V^{-1} s^{-1} and μ_h = 3.0 × 10^{-4} cm^2 V^{-1} s^{-1} for the initial **Bis-PDI-T-EG** blend). Furthermore, light-power-dependent *J*–*V* curves also indicated a decrease in both monomolecular and bimolecular recombination losses in the optimised blend, thus explaining the almost 50% larger J_{SC} and PCE of 6.08%. Over the course of a year, the OPV performance of this model donor–acceptor system was improved once again, by replacing the PBDTTT-C-T donor with the lower band gap polymer PBDT-TS1, thereby favouring photon absorption across a broader wavelength range and consequently improving the J_{SC}.[85] Incorporation of the molecular PDINO species in the Ca electron transporting layer on the other hand aided electron mobility, factor (μ_e = 1.87 × 10^{-3} cm^2 V^{-1} s^{-1} for the **Bis-PDI-T-EG** blend using a PDINO ETL *cf.* μ_e = 1.16 × 10^{-3} cm^2 V^{-1} s^{-1} for the regular **Bis-PDI-T-EG** blend) and hence the FF, which also contributes to the higher PCE of 7.24% of the devices. Concomitantly to the optimisation of **Bis-PDI-T-EG** based devices, a boost in OPV PCE was attempted through side-chain engineering of the methoxy-capped ethylene glycol units.[86] Substitution by 4-butylalkoxy moieties afforded **Bis-PDI-T-BuO**, whose side chains were envisaged to adjust the intermolecular interactions with the donor by adopting an antiperiplanar rather than gauche conformation. Moreover, the reduced flexibility of the *n*-butoxyl chains should also lead to slightly increased π–π stacking distances and therefore more suitably tuned phase domains. When blended with the same polymer donor (PBDT-TS1) as in the best performing **Bis-PDI-T-EG** device a PCE of 6.36% was obtained. The decreased performance was suggested to be a result of the excessively large aggregation of the acceptor in the active layer, leading to poor exciton dissociation therefore accounting for the reduced photocurrent. **FPDI-T** is analogous to the **Bis-PDI-T-EG** and **Bis-PDI-T-BuO** acceptors, however it contains a fully fused thiophene linker and different solubilising chains.[87] Ring fusion between the aromatic linker and the two PDI monomers was suggested to be an effective way to rigidify the PDI acceptor, thereby favouring its morphology in blends.[75] DFT calculations confirmed the success of this strategy by demonstrating a significantly decreased dihedral angle in **FPDI-T**, thereby planarising the molecule and aiding π–π stacking in OPV blends. GIWAXS reinforced this hypothesis as **FPDI-T** possessed a more intense and narrow out-of-plane π–π stacking peak. A result of the tighter molecular packing was an improved charge carrier transport, which was reflected in the excellent hole and electron mobilities (μ_e = 1.63 × 10^{-4} cm^2 V^{-1} s^{-1} and μ_h = 5.92 × 10^{-2} cm^2 V^{-1} s^{-1} for the **FPDI-T** blend). Consequently this is reflected in the high PCE of 6.72% obtained for PTB7-Th:**FPDI-T** based devices. Another high-performance PDI with a fully fused nonacyclic IDTT core, **FITP**, was presented.[88] The selection of the IDTT core was based on its extended conjugation length and strong electron-donating nature. UV-vis spectroscopy highlighted the advantages of **FITP**'s more extended aromatic backbone by showing improved photon absorption at longer wavelengths compared to **FPDI-T**. The 10% higher J_{SC} in PTB7-Th:**FITP** devices is further proof of the maximised charge generation and responsible for the improved PCE of 7.33%. An alternative aromatic bridging moiety to have shown considerable promise in bay-linked PDI dimers is 9,9′-spirobifluorene. 9,9′-Spirobifluorene was selected as a bridge in **SF-PDI$_2$** because of its helical shape and high lying LUMO, which should benefit **SF-PDI$_2$**'s morphological and optoelectronic properties respectively.[89] AFM confirmed the favourable morphology of **SF-PDI$_2$** in PffBT4T:**SF-PDI$_2$** blends revealing domain sizes around 20–30 nm. The high photoluminescence quenching efficiency of 93% suggests that well-sized donor–acceptor domains extend also beyond the surface of the film. The judiciously tuned LUMO energy of **SF-PDI$_2$** by inclusion of 9,9′-spirobifluorene was reflected in the large V_{OC} of 0.98 V obtained in the optimised solar cells with a PCE of 6.30%. Further device optimisation was performed by pairing **SF-PDI$_2$** with the low bandgap polymer P3TEA to achieve an impressive PCE of 9.50% with an at the time record V_{OC} of 1.11 V.[90] The large V_{OC} can be rationalised through the low voltage loss of only 0.61 V in the devices, the origin of

Open Access Article. Published on 26 April 2018. Downloaded on 3/28/2024 5:48:32 PM.
This article is licensed under a Creative Commons Attribution 3.0 Unported Licence.

which stems from the lack of any sub-bandgap charge transfer state absorption and minimised non-radiative recombination mechanisms. Perhaps an even more striking aspect of the photovoltaic performance data is that despite an apparently almost negligible energy offset of 0.05 eV between P3TEA and **SF-PDI$_2$**'s LUMOs, charge generation and separation remained efficient as demonstrated by the high J_{SC}. Another advantageous property of **SF-PDI$_2$** over other PDI-based NFAs is its ease of synthesis, as **SF-PDI$_2$** was obtained in three steps from the commercially available and inexpensive perylene-3,4,9,10-tetracarboxylic dianhydride. Moreover, the use of a Suzuki rather than Stille cross-coupling reaction between bis(pinacolato)spirobifluorene and the bay position monobrominated perylene diimide precursor also avoids the use of any highly toxic organotin reagents, thus further adding to **SF-PDI$_2$** industrial applicability.

3.3. PDI trimers

To mimic fullerene's spherical shape, hence its favourable isotropic charge transport, three-dimensional PDI trimers have been developed (Fig. 10). This approach was designed to also benefit the morphological properties of the donor–acceptor blend, as the constituent PDI monomers of the NFA are rotated in different directions, thereby reducing PDIs' inherent aggregation tendency. One of the earliest PDI trimers was **S(TPA-PDI)**.[91] This acceptor utilises a triphenylamine core joined to three PDI arms leading to an NFA with a star-shaped structure. Moreover, the use of

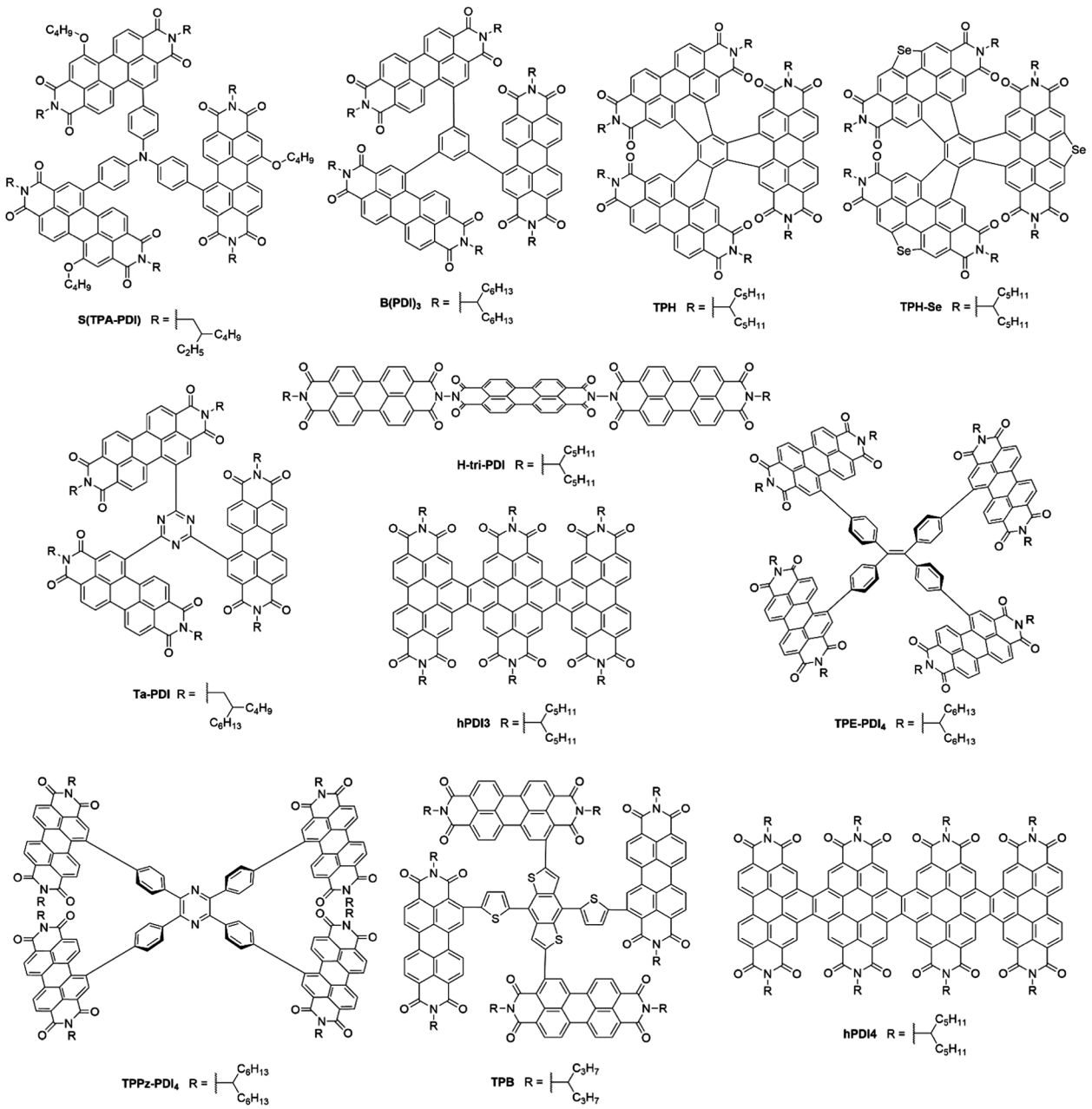

Fig. 10 Trimeric and tetrameric PDI based small molecule acceptors.

 This journal is © The Royal Society of Chemistry 2019

Open Access Article. Published on 26 April 2018. Downloaded on 3/28/2024 5:48:32 PM.
This article is licensed under a Creative Commons Attribution 3.0 Unported Licence.

Table 4 Summary of the optoelectronic properties of trimeric and tetrameric PDI based small molecule acceptors and their *J*–*V* characteristics in bulk heterojunction solar cells

Acceptor	Optical E_g (eV)	HOMO (eV)	LUMO (eV)	V_{OC} (V)	J_{SC} (mA cm^{-2})	FF	Electron mobility[a] (cm^2 V^{-1} s^{-1})	Hole mobility[b] (cm^2 V^{-1} s^{-1})	PCE[c] (%)	Donor	Additive	Ref.
S(TPA-PDI)	1.76	−5.40	−3.70	0.88	11.3	0.34	2.32×10^{-5}	7.17×10^{-4}	3.32 (3.22)	PBDTTT-C-T	5.0% DIO	91
B(PDI)$_3$	2.14	−6.00	−3.86	0.83	13.1	0.52	4.20×10^{-5}	1.75×10^{-4}	5.65 (—)	PTB7-Th	3.0% CN	92
TPH	2.19	−6.02	−3.83	1.00	12.3	0.64	1.50×10^{-3}	1.00×10^{-3}	8.28 (8.15)	PDBT-T1	0.25% DIO	93
TPH-Se	2.17	−5.97	−3.80	1.00	13.0	0.72	2.20×10^{-3}	1.70×10^{-3}	9.28 (8.98)	PDBT-T1	0.75% DIO	94
Ta-PDI	2.05	−6.03	−3.81	0.78	17.1	0.69	2.70×10^{-4}	3.60×10^{-4}	9.15 (8.91)	PTB7-Th	—	95
H-tri-PDI	2.09	−6.01	−3.93	0.73	16.5	0.60	1.40×10^{-5}	1.20×10^{-4}	7.25 (—)	PDBT-TS1	7.0% DPE	95
hPDI3	2.37	−6.23	−3.86	0.81	14.5	0.67	1.50×10^{-4}	1.00×10^{-4}	7.90 (7.70)	PTB7-Th	1.0% DIO	96
TPE-PDI$_4$	2.05	−5.77	−3.72	0.91	11.7	0.52	1.00×10^{-3}	—	5.53 (5.44)	PBDTT-S-TT	—	97
TPPz-PDI$_4$	2.10	−5.86	−3.76	0.99	12.5	0.56	2.30×10^{-3}	—	7.10 (6.90)	PffBT-T3(1,2)-2	—	98
TPB	1.82	−5.71	−3.89	0.79	17.9	0.58	6.00×10^{-6}	1.08×10^{-5}	8.47 (8.11)	PTB7-Th	8.0% DPE	99

[a] Determined by space charge limited current (SCLC) measurements using electron only devices. [b] Determined by space charge limited current (SCLC) measurements using hole only devices. [c] Average PCE values are shown in parentheses.

an electron rich central unit and electron deficient end units induces a significant push–pull character in the molecule intended to favour photon absorption across a broad range of wavelengths. When blended with the low bandgap polymer donor PBDTTT-C-T, good photovoltaic performance with a PCE of 3.32% was reported (Table 4). The main limitation of the solar cell performance was the poor FF of 0.34, which can be predominantly attributed to the poorly balanced and moderate hole and electron mobilities ($\mu_e = 2.32 \times 10^{-5}$ cm^2 V^{-1} s^{-1} and $\mu_h = 7.17 \times 10^{-4}$ cm^2 V^{-1} s^{-1} for the **S(TPA-PDI)** blend). Based on **S(TPA-PDI)**'s molecular design, **B(PDI)$_3$** was developed in which a phenyl moiety was selected as a replacement for **S(TPA-PDI)**'s triarylamine core.[92] Although substitution of the sp^3 hybridised nitrogen central unit by the more planar sp^2 hybridised phenyl group no longer afforded a star-shaped structure, a 51.4° dihedral angle (from DFT calculations using B3LYP/6-31G basis sets) between the phenyl and PDI planes ensured retention of a twisted molecular geometry, thereby suppressing PDI's strong aggregation tendency. Grazing incidence X-ray diffraction indicated crystal sizes of around 5 nm in the active layer, which in turn benefited J_{SC}. Short π–π stacking distances around 1.5 nm for both the PTB7-Th donor and the **S(TPA-PDI)** acceptor were also found, consequently allowing for the formation of good charge-transport networks, which is highlighted in the almost 50% improved FF of PTB7-Th:**B(PDI)$_3$** devices compared to **S(TPA-PDI)** based cells. Devices spin-casted from a PTB7-Th:**B(PDI)$_3$** blend ultimately yielded a PCE of 5.65%. In an attempt to further exploit the structurally favourable properties of the benzene core, two novel C_3 symmetric NFAs, **TPH** and **TPH-Se**, were designed.[93] In comparison to **B(PDI)$_3$**, these acceptors featured a fully-annulated aromatic core, which was achieved through a Pd-catalysed Suzuki cross-coupling followed by subsequent photocyclization. The aim of this modification was to generate a highly delocalised π-system to confer intense photon absorption as well as favourable charge carrier mobilities. Solar cells for **TPH** and **TPH-Se** were fabricated from PDBT-T1:NFA blends, yielding impressive performances with a PCE of 8.28% and 9.28% respectively. The notable photovoltaic performance of both devices was attributed to the stronger and broader optical absorption of both acceptors compared to **S(TPA-PDI)** and **B(PDI)$_3$** and the ideally-sized domains in both donor–acceptor combinations (14.70 nm and 14.20 nm for **TPH** and **TPH-Se** respectively), as indicated by resonant soft X-ray scattering (R-SoXS). It was speculated that the tighter molecular packing in **TPH-Se** arising from increased Se–Se interactions in neighbouring molecules accounts for the slightly higher and more balanced electron and hole mobilities in PDBT-T1:**TPH-Se** compared to PDBT-T1:**TPH** thus also the superior FF and photovoltaic performance ($\mu_e = 2.2 \times 10^{-3}$ cm^2 V^{-1} s^{-1} and $\mu_h = 1.7 \times 10^{-3}$ cm^2 V^{-1} s^{-1} for the **TPH-Se** blend *cf.* $\mu_e = 1.5 \times 10^{-3}$ cm^2 V^{-1} s^{-1} and $\mu_h = 1.0 \times 10^{-3}$ cm^2 V^{-1} s^{-1} for the **TPH** blend) (Fig. 11).

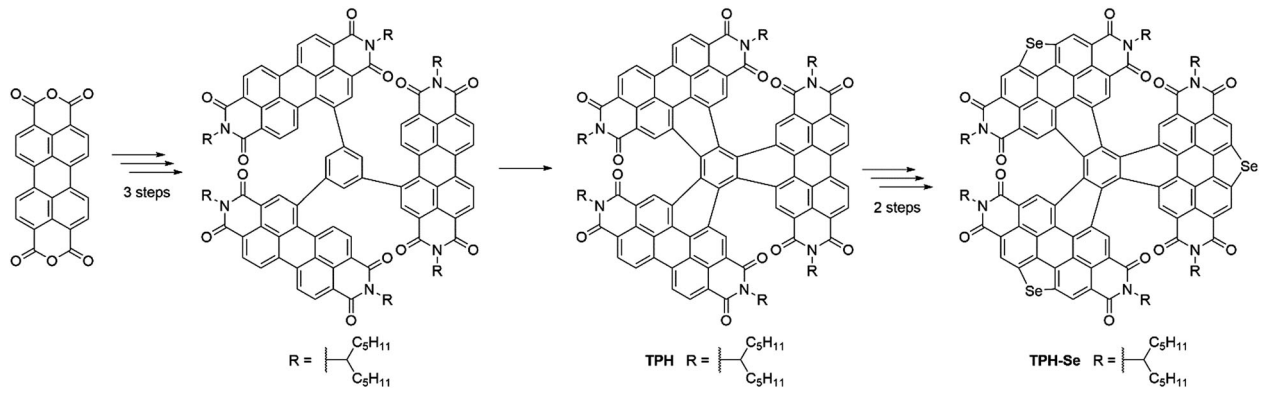

Fig. 11 Synthetic routes employed for **TPH** and **TPH-Se** involving photocyclization to achieve a fully-annulated aromatic core.

Open Access Article. Published on 26 April 2018. Downloaded on 3/28/2024 5:48:32 PM.
This article is licensed under a Creative Commons Attribution 3.0 Unported Licence.

Whilst each of the previously discussed trimeric PDI NFAs employ an electron-donating central building block, the first PDI derivative containing an electron-deficient core, **Ta-PDI**, was recently reported.[94] Due to the electron-poor nature of the triazine π-bridge, an inversion of the typical arrangement of the halide and organometallic functionalities on the PDI and aromatic linker coupling partners used in the Pd-catalysed cross-coupling reaction of **Ta-PDI** was needed, thus setting a synthetic precedent for future PDI oligomers with electron-poor cores. Inverted architecture OPV devices were spin-casted from a PTB7-Th:**Ta-PDI** blend to yield an outstanding photovoltaic performance with PCE of 9.15%. Although using a different donor, **Ta-PDI** based devices yielded a significantly higher J_{SC} of 17.1 mA cm^{-2} than each of the previously discussed trimeric PDI NFAs, which can be related to its higher EQE of almost 80% across a broad spectral range. Furthermore, the impressive J_{SC} can be attributed to efficient exciton dissociation as indicated by charge dissociation probability $P(E,T)$ measurements, yielding a value of 98%. The V_{OC} of PTB7-Th:**Ta-PDI** devices on the other hand was significantly below those of devices fabricated from the other trimeric acceptors, which can be attributed to the electron-withdrawing nature of the triazine core downshifting the LUMO of the acceptor (Fig. 12).

Following previous work on imine coupled PDI monomers, the trimeric N-linked PDI non-fullerene acceptor, **H-tri-PDI** was designed.[75,95] Whilst it was envisaged that the inclusion of an additional PDI unit in the acceptor would enhance photon absorption, thereby benefiting J_{SC} in the devices, retention of the 90° dihedral angle between the PDI planes (estimated using DFT calculations with the B3LYP/6-31G* basis sets) should continue to disrupt the acceptor's aggregation tendency and favour the blend morphology. The success of this design strategy is reflected in the R-SoXS data of PBDT-TS1:**T-tri-PDI** blends, which indicates characteristic mode length scales in the order of 15 nm. These findings also account for the remarkable J_{SC} of 16.5 mA cm^{-2} in the champion PBDT-TS1:**H-tri-PDI** devices with a PCE of 7.25%. Another example of improved photovoltaic performance upon inclusion of an additional repeat unit in a PDI dimer is **Helical PDI 1** and its trimeric analogue, **hPDI3**.[82,96] Similar to **Helical PDI 1**, **hPDI3** was synthesised by fusing three PDI units together at their bay positions with ethylene bridging units. Whilst both **Helical PDI 1** and **hPDI3** display nonplanar structures due to the steric congestion at their *ortho* positions, DFT calculations demonstrated that **hPDI3** can exist as two isoenergetic conformers by inversion of its helicity at either two-carbon junction. Because of these conformational dynamics and the 3D molecular structure, PTB7-Th:**hPDI3** blends exhibit highly-favourable intercalating donor–acceptor networks of approx. 20 nm in size. In combination with PTB7-Th and **hPDI3**'s excellent spectral complementarity this led to an excellent J_{SC} of 14.5 mA cm^{-2} which contributes to the devices' high PCE of 7.90%.

3.4. PDI tetramers

The structurally most complex and most recently developed class of PDI based NFAs are PDI tetramers. Amongst the early examples of these molecules was **TPE-PDI$_4$**.[97] Because of steric clashes the four phenyl rings in **TPE-PDI$_4$**'s tetraphenylethylene core are twisted by approx. 55° relative to the plane of the central double bond, thereby conferring **TPE-PDI$_4$** a four-wing propeller shaped molecular structure. This highly twisted conformation ensures good solvent processability in common organic solvents, as well as the formation of smooth thin films with a root-mean square roughness of 0.207 nm as confirmed by X-ray diffraction measurements. AFM measurements support the favourable active layer morphology, as PTB7-Th:**TPE-PDI$_4$** blends demonstrate average surface features between 20–30 nm in size. The 55° torsional angle in **TPE-PDI$_4$**'s core (estimated from DFT calculations using B3LYP/6-31G* basis sets) also ensures minimal conjugation between the four PDI units in the acceptor, which in turn leads to a high lying LUMO thus accounting for the remarkable V_{OC} of 0.91 V in the OPV devices. Ultimately, champion devices yielded a PCE of 5.53%. In a recent study, **TPE-PDI$_4$**'s central tetraphenylethylene moiety was replaced by a tetraphenylpyrazine unit to afford **TPPz-PDI$_4$**.[98] It was hypothesised that **TPPz-PDI$_4$**'s larger core should reduce steric clashes between the four phenyl units, therefore reduce the extent of molecular twisting and thereby favouring charge carrier mobilities. The success of this design strategy is reflected in DFT calculations (using B3LYP/6-31G* basis sets), which revealed a 40° dihedral angle between **TPPz-PDI$_4$**'s pyrazine and phenyl units

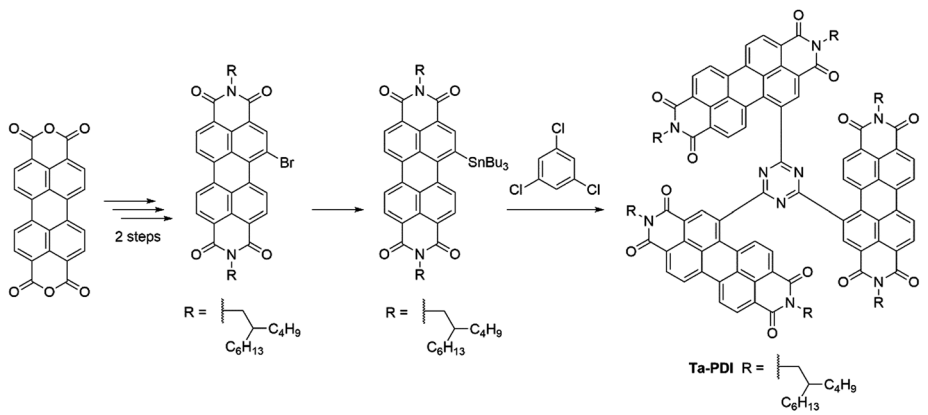

Fig. 12 Synthetic route employed for **Ta-PDI** including inversion of the halide and organometallic coupling functionalities on the PDI and aromatic core.

Open Access Article. Published on 26 April 2018. Downloaded on 3/28/2024 5:48:32 PM.
This article is licensed under a Creative Commons Attribution 3.0 Unported Licence.

(*cf.* 55° dihedral angle between **TPE-PDI$_4$**'s ethylene and phenyl groups). Space-charge-limited current electron mobility measurements also highlighted the positive outcome of the molecular engineering strategy as **TPPz-PDI$_4$** had an electron mobility more than double of **TPE-PDI$_4$** ($\mu_e = 2.3 \times 10^{-3}$ cm^2 V^{-1} s^{-1} for the **TPPz-PDI$_4$** blend *cf.* $\mu_e = 1.0 \times 10^{-3}$ cm^2 V^{-1} s^{-1} for the **TPE-PDI$_4$** blend). Devices based on PffBT-T3(1,2)-2:**TPPz-PDI$_4$** thus afforded improved photovoltaic performance compared to PTB7-Th:**TPE-PDI$_4$**, with a FF of 0.56 and PCE of 7.10%. In contrast to the minimal conjugation between PDI units in **TPE-PDI$_4$**, a benzodithiophene-thienyl (BDT-Th) molecular backbone was utilised in **TPB**, whereby the two PDI caps flanking the BDT core possessed dihedral angles of 50.2° and 58.9° respectively, hence a twist angle of 9° between the PDI groups, estimated from DFT calculations using B3LYP/6-31G(d).[97,99] This led to almost parallel equatorial PDI moieties and therefore a partially conjugated PDI–BDT–PDI backbone, which was envisaged to favour exciton splitting. Specifically, during charge transfer from the donor (PTB7-Th) to a PDI unit in the acceptor the transmitted electron can be delocalised to the opposite PDI unit thereby reducing the electron–hole binding energy. This hypothesis was supported by photoluminescence data, which showed almost completely quenched PTB7-Th and **TPB** luminescence, thus suggesting efficient charge separation. Alongside suitable donor–acceptor domain sizes and intense absorption across the entire visible spectrum, this rationalises the excellent photovoltaic performance of PTB7-Th:**TPB** blends with a PCE of 8.47%.

Overall, a range of molecular engineering strategies have been developed over the past decade to optimise both the optoelectronic and morphological properties of PDI based acceptors in OPVs, leading to PCEs as high as 9.50%. Whilst initial design concepts relied predominantly on the inclusion of electron-donating moieties between two or more PDI units, in recent years examples of oligomeric PDI acceptors with electron neutral or electron withdrawing π-bridges have also demonstrated considerable promise as NFAs in OPVs. The industrial scalability of PDI NFAs is helped by the commercial availability of the perylene tetracarboxylic dianhydride precursor, thus reducing the synthesis of some PDI NFAs to just three steps. Reports of PDI based devices processed from non-chlorinated solvents have also been rather scarce, thus requiring further attention from the OPV community to allow PDI based solar cells to become industrially viable.

4. Acceptor polymers

The first OPV device employing a polymer acceptor was developed in 1995 and utilised poly(*p*-phenylenevinylene) derivatives as both the donor and the acceptor.[100] Although no power conversion efficiencies were reported, these findings illustrated that all-polymer solar cells not only possess suitable interfaces for charge separation but also percolating networks for charge transport. Numerous classes of polymeric NFAs have since been developed, the most promising include polymeric naphthalene diimide (PNDI) acceptors, polymeric PDI (PPDI) acceptors and terpolymer acceptors (Fig. 13). The general structure of polymer NFAs relies on alternating electron-donating and electron-accepting moieties. Similar to their small molecule counterparts, the energy levels of polymeric NFAs can also be adjusted through chemical modification of both the donor and acceptor units. The inherent polydispersity of polymer NFAs, typically resulting in a distribution of molecular weights, often complicates analysis of the performance of devices and impedes the ability to reliably produce identical batches of the acceptors. Furthermore, the morphology of all-polymer bulk heterojunctions is often difficult to optimize as a result of the unfavourable mixing of two polymeric components. For this reason, progress in polymer acceptors currently lags that of small molecules. However, polymers exhibit excellent flexibility, toughness, processability and continually improving performance that encourages further development and holds promise for potential commercialisation.

4.1. Polymeric naphthalene diimide acceptors

The development of the first PNDI NFA, **P(NDI2OD-T2)**, was in 2009, where the low-lying LUMO of −3.9 eV accounted for its excellent stability under ambient conditions.[101] The synthesis of **P(NDI2OD-T2)** required bromination of the commercially available 1,4,5,8-naphthalenetetracarboxylic dianhydride at the 2 and 6 positions, followed by imidisation using 2-octyldodecan-1-amine and lastly polymerisation with 5,5′-bis(trimethylstannyl)-2,2′-bithiophene. Although organic field effect transistor (OFET) data was reported, no OPV devices were fabricated. Two years later, two independent studies reported OPV data for P3HT:**P(NDI2OD-T2)** blends yielding PCEs of 0.21% and 0.17% respectively (Table 5).[102,103] Although in both cases high electron mobilities and broad spectral coverages were reported, scanning transmission X-ray (STXM) microscopy revealed excessively large phase domains between 200–1000 nm in size, which accounted for the poor exciton dissociation and low photocurrent. Subsequent investigations were directed towards reducing **P(NDI2OD-T2)s'** aggregation tendency in blends.[104] Scanning near-field optical microscopy and AFM demonstrated that by employing solvents with large and polarisable aromatic cores, **P(NDI2OD-T2)**'s phase domains in the active layer can be significantly decreased consequently leading to an improved J_{SC} of 3.77 mA cm^{-2} and a PCE of 1.40%. The next OPV performance improvement from **P(NDI2OD-T2)** based devices was achieved by blending **P(NDI2OD-T2)** with a low bandgap polymer, PTQ1.[105] Better donor–acceptor spectral complementarity and photoluminescence quenching efficiencies of 96% for PTQ1 and 77% for **P(NDI2OD-T2)** ensured good charge generation thus accounting for the more than doubled J_{SC} and PCE of 4.10%. Further OPV performance optimisation was conducted in 2016 to afford a then highest reported efficiency for OPVs utilising polymeric NFAs.[106] The design strategy also relied on donor-polymer substitution, however rather than opting for a lower bandgap polymer, it was hypothesised that a medium bandgap donor should allow for better spectral complementarity with the low bandgap **P(NDI2OD-T2)** acceptor. In the search for the ideal donor, a fluorine substituted backbone was chosen as a critical attribute to lower the polymer's HOMO, which in

Open Access Article. Published on 26 April 2018. Downloaded on 3/28/2024 5:48:32 PM.
This article is licensed under a Creative Commons Attribution 3.0 Unported Licence.

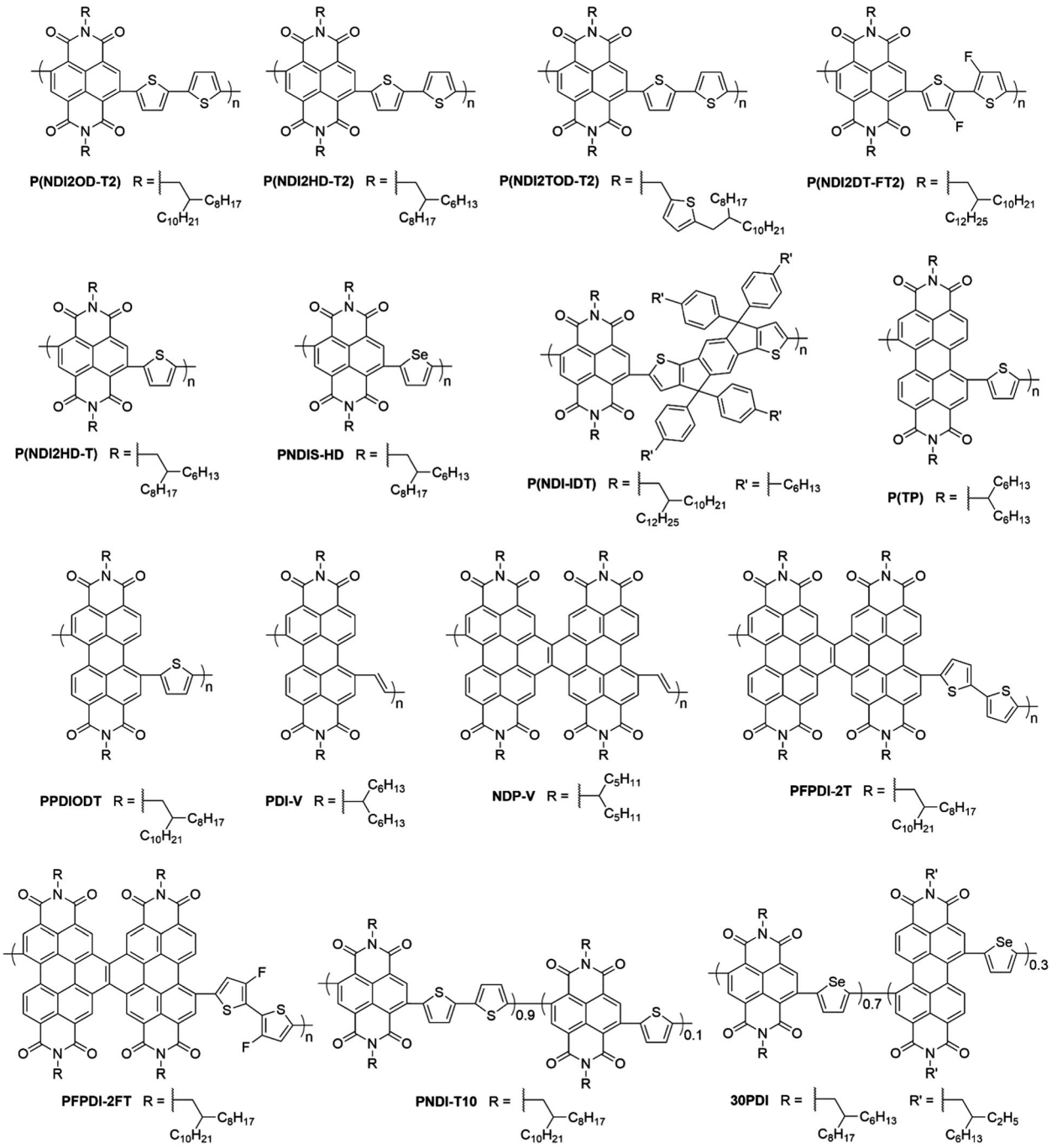

Fig. 13 NDI and PDI based polymeric acceptors.

turn should afford a larger V_{OC}. With these design criteria in mind, the bifluorinated-benzodithiophene-*alt*-benzotriazole copolymer, J51 was selected. Utilising a previously reported device configuration, solar cells were fabricated from J51:**P(NDI2OD-T2)** with a PCE of 8.27%.[106] Although both of the initial design strategies proved to be successful, leading to maximised J_{SC} and V_{OC}, an unexpectedly large FF of 0.70 also significantly contributed to the high OPV performance. The excellent FF was ascribed to the high and well-balanced charge carrier mobilities (μ_e = 2.16 × 10^{-4} cm^2 V^{-1} s^{-1} and μ_h = 2.50 × 10^{-4} cm^2 V^{-1} s^{-1} for the J51:**P(NDI2OD-T2)** blend). Very recently, an unprecedented efficiency of 10.1% for all-polymer solar cells by blending a novel wide-bandgap donor, PTzBI-Si, with **P(NDI2OD-T2)** was reported.[107] Although the resulting devices showed slightly higher V_{OC}, J_{SC} and FF compared to previously reported cells, a more remarkable aspect of these findings was the fact that a record PCE was obtained by spin-coating devices from a non-chlorinated solvent, 2-methyl-tetrafuran, whereby the outstanding solution processability of the new polymer donor was linked to its siloxane capped alkyl chains.

Open Access Article. Published on 26 April 2018. Downloaded on 3/28/2024 5:48:32 PM. This article is licensed under a Creative Commons Attribution 3.0 Unported Licence.

Table 5 Summary of the optoelectronic properties of NDI and PDI based polymeric acceptors and their J–V characteristics in bulk heterojunction solar cells

Acceptor	Optical E_g (eV)	HOMO (eV)	LUMO (eV)	V_{OC} (V)	J_{SC} (mA cm^{-2})	FF	Electron mobility[a] (cm^2 V^{-1} s^{-1})	Hole mobility[b] (cm^2 V^{-1} s^{-1})	PCE[c] (%)	Donor	Additive	Ref.
P(NDI2OD-T2)	1.45	−5.45	−4.00	0.52	1.41	0.29	—	—	0.21 (—)	P3HT	—	102
P(NDI2OD-T2)	1.45	−5.45	−4.00	0.46	0.80	0.46	—	—	0.17 (—)	P3HT	—	103
P(NDI2OD-T2)	1.45	−5.80	−4.35	0.56	3.77	0.65	—	—	1.40 (—)	P3HT	—	104
P(NDI2OD-T2)	1.60	−5.90	−4.30	0.84	8.85	0.55	2.70×10^{-3}	1.20×10^{-5}	4.10 (4.00)	PTQ1	—	105
P(NDI2OD-T2)	1.48	−5.77	−3.84	0.83	14.18	0.70	2.16×10^{-4}	2.50×10^{-4}	8.27 (8.10)	J51	1.0% DIO	106
P(NDI2OD-T2)	1.46	−5.81	−3.84	0.87	15.57	0.73	2.88×10^{-4}	1.87×10^{-3}	10.10 (9.90)	PTz-BI-Si	—	107
P(NDI2HD-T2)	1.47	—	—	0.82	13.97	0.53	6.23×10^{-5}	9.79×10^{-5}	6.11 (6.03)	PTB7-Th	—	108
P(NDI2TOD-T2)	1.43	−5.36	−3.93	0.77	11.40	0.54	2.20×10^{-5}	6.10×10^{-5}	4.75 (—)	PTB7-Th	3.0% DPE	109
P(NDI2DT-FT2)	—	—	—	0.81	13.53	0.62	4.90×10^{-4}	5.50×10^{-4}	6.71 (6.58)	PTB7-Th	—	110
P(NDI2HD-T)	1.85	−5.64	−3.79	1.06	11.22	0.56	1.55×10^{-5}	2.84×10^{-5}	6.64 (6.60)	PBDTTTPD	1.0% DIO	111
PNDIS-HD	1.65	−5.65	−4.00	0.76	7.78	0.55	1.00×10^{-3}	2.00×10^{-4}	3.26 (3.16)	PSEHTT	—	112
PNDIS-HD	1.76	−6.00	−3.84	0.81	18.80	0.51	7.25×10^{-3}	3.11×10^{-4}	7.73 (7.21)	PTB7-Th	—	113
P(IDT-NDI)	1.51	−5.75	−3.84	0.93	9.55	0.60	3.06×10^{-5}	6.58×10^{-5}	5.33 (5.19)	J51	—	114
P(TP)	1.80	−5.72	−3.8	0.98	9.97	0.51	1.25×10^{-4}	8.00×10^{-5}	5.00 (4.88)	Pil-2T-PS-10	2.0% MN	115
PPDIODT	1.74	−5.90	−3.96	0.76	15.72	0.55	1.71×10^{-3}	5.75×10^{-4}	6.58 (6.50)	PBDT-TS1	—	116
PDI-V	1.74	−5.77	−4.03	0.74	15.80	0.63	4.20×10^{-4}	1.30×10^{-3}	7.57 (7.30)	PTB7-Th	—	117
NDP-V	1.91	−5.94	−4.03	0.74	17.07	0.67	3.00×10^{-4}	1.00×10^{-3}	8.59 (8.48)	PTB7-Th	—	118
PFPDI-2T	1.70	−5.82	−4.12	0.73	13.47	0.65	3.84×10^{-5}	2.67×10^{-4}	6.39 (6.31)	PTB7-Th	3.0% CN	119
PFPDI-2FT	1.79	−5.94	−4.15	0.67	13.31	0.60	3.32×10^{-5}	2.32×10^{-4}	5.35 (5.26)	PTB7-Th	3.0% CN	119
PNDI-T10	1.55	−6.36	−4.05	0.89	12.30	0.63	2.70×10^{-5}	7.80×10^{-5}	6.90 (6.60)	PBDTTS-FTAZ	—	120
PNDI-T10	1.55	−6.36	−4.05	0.83	12.90	0.71	6.00×10^{-4}	1.00×10^{-3}	7.60 (7.40)	PTB7-Th	—	121
30PDI	1.77	−5.95	−3.89	0.79	18.55	0.45	1.00×10^{-3}	2.60×10^{-3}	6.29 (6.17)	PBDTTT-C-T	3.0% DIO	122

[a] Determined by space charge limited current (SCLC) measurements using electron only devices. [b] Determined by space charge limited current (SCLC) measurements using hole only devices. [c] Average PCE values are shown in parentheses.

Having demonstrated the potential of PNDI NFAs and successfully optimised initial devices based on **P(NDI2OD-T2)**, the focus of the OPV community shifted to molecular design strategies to ameliorate the performance of PNDI NFAs. Early approaches sought to improve the crystalline behaviour and molecular orientation of **P(NDI2OD-T2)** by varying the length of its pendant alkyl chains. In a series of PNDI NFAs, the 2-hexyldecyl substituted **P(NDI2HD-T2)** afforded the highest photovoltaic performance with a PCE of 6.11% when blended with PTB7-Th.[108] Notably, the PTB7-Th:**P(NDI2HD-T2)** combination had a superior efficiency compared to the PTB7-Th:**P(NDI2OD-T2)** reference, which was ascribed to **P(NDI2HD-T2)**'s higher and more balanced hole and electron mobilities as well as a more-intermixed and finer blend morphology ($\mu_e = 6.18 \times 10^{-5}$ cm^2 V^{-1} s^{-1} and $\mu_h = 9.79 \times 10^{-5}$ cm^2 V^{-1} s^{-1} for the **P(NDI2HD-T2)** blend *cf.* $\mu_e = 1.31 \times 10^{-5}$ cm^2 V^{-1} s^{-1} and $\mu_h = 5.71 \times 10^{-5}$ cm^2 V^{-1} s^{-1} for the **P(NDI2OD-T2)** blend). These findings thus suggest that tuning the side chains of PNDIs is a simple, yet effective strategy to enhance their OPV performance. Based on this observation, **P(NDI2TOD-T2)** was developed, in which the introduction of alkyl-thiophene pendant groups onto the NDI–bithiophene backbone was intended to promote intermolecular interactions.[109] The success of this strategy is highlighted by the slightly broader absorption spectra in thin films compared to the **P(NDI2OD-T2)** reference, as well as the reduced packing distance in blends with PTB7-Th, indicating stronger intermolecular interactions. Although the PTB7-Th:**P(NDI2TOD-T2)** cells yielded a PCE of 4.75% and marginally outperformed the **P(NDI2OD-T2)** reference, they were unable to reach the state of the art PTB7-Th:**P(NDI2HD-T2)** devices. Another layer of complexity to earlier work was added by the introduction of additional fluorine substituents on the polymer backbone, resulting in **P(NDI2DT-FT2)** acceptor.[110] The presence of electron-withdrawing substituents was not only intended to affect the FMOs, but also induce higher molecular organisation to promote higher charge-carrier mobilities. A maximum PCE of 6.71% was reported for the PBDTT-F-T:**P(NDI2DT-FT2)** blend, outperforming the PBDTT-F-T:**P(NDI2OD-T2)** reference by more than 25%. AFM and GIWAXS suggested that this was due to the preferential formation of fibrillar nanostructures and face-on stacking in the former blend, both favouring charge carrier transport. These findings corroborate well with the enhanced FF and J_{SC} in the PBDTT-F-T:**P(NDI2DT-FT2)** devices.

Substitution of the bithiophene monomer by alternative aromatic moieties to modulate the electron density on the polymer and improve device efficiency have also been explored. Following this design principle the NDI–thiophene copolymer **P(NDI2HD-T)** was developed.[111] The selection of a thiophene donor unit was based on its tendency to disrupt NDI's strong aggregation tendency, a result of the large dihedral angles between the thiophene and PDI planes, whilst retaining similar electron donating properties to bithiophene. Cells fabricated from blends of PBDTTTPD:**P(NDI2HD-T)** afforded a noteworthy PCE of 6.64%. R-SoXS measurements and AFM indicated small and well-intermixed phase domains thus highlighting the success of the molecular engineering strategy employed. To further boost performance, **P(NDI2HD-T)**'s selenium analogue, **PNDIS-HD** was synthesised.[112] It was hypothesised that the incorporation of a selenium atom would improve orbital overlap between the heteroatom and the aromatic system, thus enhance the charge carrier mobilities. Moreover, Se–Se interactions were also envisaged to increase the crystallinity of the polymer, thereby improve phase separation in blends. Although initial devices only yielded <4%

Open Access Article. Published on 26 April 2018. Downloaded on 3/28/2024 5:48:32 PM.
This article is licensed under a Creative Commons Attribution 3.0 Unported Licence.

efficiencies, subsequent device optimisation by tuning the donor polymer and the rate of polymer/polymer self-organisation afforded devices with a higher PCE of 7.70%.[113] A structurally more complex PNDI, **P(NDI-IDT)**, was designed and consists of alternating NDI and IDT units.[114] The IDT core was selected due to its rigidity and coplanarity, which was expected to favour charge carrier mobilities. Moreover, the presence of four hexylphenyl solubilising groups on the IDT backbone was intended to give rise to excellent solution processability and suppress the polymer's aggregation tendency in the solid state. Devices were fabricated by spin-coating J51:**P(IDT-NDI)** blends onto ITO substrates affording a PCE of 5.33%. Considering that the difference between the HOMO of the donor and the LUMO of the acceptor is only ~1.6 eV, a relatively high V_{OC} of 0.93 V was obtained. In combination with well-sized phase domains in the active blend, featuring a root mean square roughness of 2.09 nm, this explains the satisfactory photovoltaic performance.

4.2. Polymeric perylene diimide acceptors

P(TP) is similar to **P(NDI2HD-T)** in that it also employs a thiophene co-monomer, however rather than an NDI acceptor subunit, it includes PDI instead.[115] Substitution of NDI by the sterically more hindered PDI resulted in an increased dihedral angle of 60° (estimated from DFT calculations using B3LYP/6-31G*) across the thiophene–PDI bond, which in turn led to a more twisted and less crystalline structure. The introduction of dove-tailed 1-hexylheptyl chains at the imide positions of **P(TP)** was designed to further hinder the self-aggregation tendency of the PDI units, thus giving rise to excellent solution processability. Devices were prepared by spin-coating PiI-2T-PS10:**P(TP)** solutions in toluene onto ITO substrates and a PCE of 5.0% was achieved. The use of a non-chlorinated processing solvent during device fabrication compensates for the only moderate performance, as this would potentially allow for the industrial upscaling of solar cells utilizing this NFA. A similar PPDI to **P(TP)**, namely **PPDIODT**, was reported in which the 1-hexylheptyl pendant chains were replaced by more extended 2-octyldodecyl chains to further boost solubility in environmentally benign solvents.[116] Champion devices based on **PPDIODT** were cast from anisole solution and outperformed **P(TP)** devices by more than 20%. The smaller phase domains, ~25 nm in the active layer of **PPDIODT** cells, compared to ~50 nm in **P(TP)** cells led to significantly improved exciton splitting and subsequently improved short circuit current. It was suggested that one of the key factors limiting the efficiencies in the previously mentioned PPDI-based devices was the excessive backbone twist in the PPDIs' backbones thus resulting in poor polymer crystallinity and low electron mobilities. With this design guideline in mind, the thiophene co-monomer was replaced by a vinylene linker to afford **PDI-V**.[117] DFT calculations, using B3LYP/6-31G* basis sets, showed a significantly decreased dihedral angle of only ~5° and GIWAXS confirmed the structural regularity of the polymer backbone. The success of this design strategy was ultimately highlighted by the more than 30% higher fill factor in PTB7-Th:**PDI-V** devices, yielding an improved PCE of 7.11%.

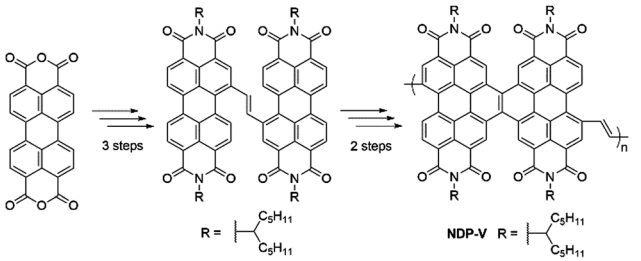

Fig. 14 Synthetic routes employed for **NDP-V** cyclization to achieve an annulated aromatic core.

In a recent elaboration, half of **PDI-V**'s vinylene units were covalently fused to the bay region of the adjacent PDI cores thus affording a naphthodiperylenetetraimide-vinylene based polymer, **NDP-V** (Fig. 14).[118] The resulting larger aromatic repeat unit and fewer twistable C–C bonds were intended to further boost the acceptor's crystallinity and lead to a more favourable blend morphology. Space charge limited current measurements revealed 50% higher charge carrier mobilities for PTB7-Th:**NDP-V** blends compared to the PTB7-Th:**PDI-V** reference ($\mu_e = 3.0 \times 10^{-4}$ cm^2 V^{-1} s^{-1} and $\mu_h = 1.0 \times 10^{-3}$ cm^2 V^{-1} s^{-1} for the **NDP-V** blend *cf.* $\mu_e = 2.0 \times 10^{-4}$ cm^2 V^{-1} s^{-1} and $\mu_h = 7.6 \times 10^{-4}$ cm^2 V^{-1} s^{-1} for the **PDI-V** blend), thereby partially explaining the improved FF in **NDP-V** based cells. It was speculated that a slightly higher root-mean-square roughness in PTB7-Th:**NDP-V** further aided charge collection, hence the FF. Ultimately, PTB7-Th:**NDP-V** devices achieved an impressive PCE of 8.59%. Another outstanding finding in this work was the retention of PCEs in excess of 8% whilst employing four different solubilising alkyl chains, suggesting that the material morphology is almost entirely dictated by the polymer backbone. Despite these successes, one of the drawbacks of **NDP-V** is its lengthier and more challenging synthesis compared to structurally more simple polymeric NFAs, such as **P(NDI2OD-T2)**, thus potentially posing an issue for its industrial scale-up. Inspired by the naphthodiperylenetetraimide core, two further acceptors combining this unit once with bithiophene and once with difluorobithiophene were designed to afford **PFPDI-2T** and **PFPDI-2FT** respectively.[117,119] Bithiophene was chosen as a suitable donor unit because of its electron-rich nature, which in turn should lead to a narrower bandgap and improved photon absorption. The two fluorine atoms on difluorobithiophene on the other hand were envisaged to aid exciton splitting by increasing the HOMO–HOMO offset between the donor and the acceptor whilst also favouring greater backbone planarity through S···F dipolar interactions. When combining **PFPDI-2T** and **PFPDI-2FT** with the low bandgap polymer PTB7-Th maximum PCEs of 6.39% and 5.35% were obtained respectively, meaning that neither acceptor was able to outperform the previously reported similar NFAs.[117,118] The reduced J_{SC} of ~13 mA cm^{-2} in both sets of devices was the primary cause for the lower efficiency and was attributed to the larger root-mean-square roughness >1.00 nm leading to excessively large domain sizes in the active layer resulting in increased charge recombination.

Open Access Article. Published on 26 April 2018. Downloaded on 3/28/2024 5:48:32 PM. This article is licensed under a Creative Commons Attribution 3.0 Unported Licence.

4.3. Terpolymer acceptors

A key factor limiting the performance of polymeric acceptors in organic photovoltaics is their low fill factor arising from their unbalanced charge carrier mobilities and suboptimal blend morphologies. As discussed previously, significant efforts have been devoted to the molecular engineering of the polymer backbone and side chains, as well as judicious tuning of device processing conditions to overcome these limitations. A more recent strategy to tackle these issues is based on the copolymerisation of multiple existing building blocks, which should allow for a more predictable tuning of the chemical and physical properties. By varying the monomer ratio during the synthesis, careful control over the frontier molecular energy levels, charge transport and film morphology is expected. One of the frontrunning polymers employing this strategy in the context of polymeric NFAs was **PNDI-T10**, a random ternary polymer comprised of an NDI acceptor unit and a 1 : 9 ratio of thiophene and bithiophene donor moieties.[120] The inclusion of thiophene in the polymer backbone was intended to increase its flexibility by reduction of the chain regularity and the increased torsional angle around the NDI–thiophene linkage. In combination with the high bandgap polymer donor PBDTT-FTAZ, an impressive PCE of 6.9% was achieved. Most notably, the performance of **PNDI-T10** was superior to devices of both binary reference polymers **PNDI-T** and **P(NDI2OD-T2)**, therefore highlighting the success of this molecular engineering approach. Whilst space charge limited current measurements showed a more balanced hole and electron mobility in **PNDI-T10** devices thus explaining its higher fill factor ($\mu_e = 2.7 \times 10^{-5}$ cm^2 V^{-1} s^{-1} and $\mu_h = 7.8 \times 10^{-5}$ cm^2 V^{-1} s^{-1} for the **PNDI-T10** blend *cf.* $\mu_e = 6.8 \times 10^{-6}$ cm^2 V^{-1} s^{-1} and $\mu_h = 4.2 \times 10^{-5}$ cm^2 V^{-1} s^{-1} for the **PNDI-T** blend and $\mu_e = 1.1 \times 10^{-5}$ cm^2 V^{-1} s^{-1} and $\mu_h = 8.9 \times 10^{-5}$ cm^2 V^{-1} s^{-1} for the **P(NDI2OD-T2)** blend), AFM indicated more carefully tuned phase domains in the active layer leading to improved charge generation. Additional device optimisation was performed and involved replacing PBDTT-FTAZ with the narrow bandgap polymer PTB7-Th.[121] Interestingly, although polymer substitution deteriorated the spectral complementarity of the active layer, J_{SC} remained largely unaffected. External quantum efficiency measurements suggested that this is because of the much-improved photon-to-electron conversion at longer wavelengths, primarily due to PTB7-Th's lower bandgap compared to PBDTTs-FTAZ. The improved performance could therefore be attributed to the more than 15% higher FF of 0.71 in the PTB7-Th:**PNDI-T10** devices, which stems from the more than 10-fold greater and more balanced charge carrier mobilities ($\mu_e = 6.0 \times 10^{-4}$ cm^2 V^{-1} s^{-1} and $\mu_h = 1.0 \times 10^{-3}$ cm^2 V^{-1} s^{-1} for the PTB7-Th:**PNDI-T10** blend *cf.* $\mu_e = 2.7 \times 10^{-5}$ cm^2 V^{-1} s^{-1} and $\mu_h = 7.8 \times 10^{-5}$ cm^2 V^{-1} s^{-1} for the PBDTTs-FTAZ:**PNDI-T10** blend).

Rather than using two different electron-rich monomers and one electron-poor monomer, a series of polymers from a single donor monomer, selenophene, and two different acceptor monomers, NDI and PDI, was synthesised.[122] The aim of this molecular engineering strategy was to attain an optimum blend morphology by varying the ratio of the more crystalline NDI-selenophene and more amorphous PDI-selenophene repeat units. When blended with PBDTTT-C-T it was found that the polymer containing 30% PDI-selenophene repeat units, **30PDI**, gave the highest efficiency with a maximum PCE of 6.29%. A particularly impressive feature of the devices was their J_{SC} of 18.55 mA cm^{-2}, so-far the highest reported J_{SC} for all-polymer solar cells. This property was attributed to the average crystalline domain sizes of 5.11 nm that closely match the typical exciton diffusion length $\sim$5 nm in OPVs. The main factor still limiting device performance was the poor FF of 0.45 arising from severe recombination losses, partially due to the insufficient phase segregation, resulting in the absence of fibrillar donor:acceptor networks that are known to facilitate charge separation and transport.

In summary, most of the research efforts in polymeric NFAs have been dedicated towards optimising the PCE of **P(NDI2OD-T2)** based OPVs due to **P(NDI2OD-T2)**'s favourably tuned energy levels, high charge carrier mobilities and facile synthesis. Despite systematically investigating the effects of the solubilising groups and the electron rich co-monomer in this model system, the so-far highest reported PCE for all-polymer solar cells has been reported for the reference **P(NDI2OD-T2)** system, thus indicating that increases in structural complexity are not always a necessity nor a guarantee for higher PCEs in OPVs. To overcome the limitations posed by PNDIs' highly crystalline nature, two alternative polymeric NFA classes have been developed. In PPDIs the increased steric bulk of the PDI moiety is used to reduce the backbone planarity by favouring larger dihedral angles around the linkages connecting the two monomers. Morphology control in terpolymers on the other hand is achieved by the variation of the nature and stoichiometry of the chosen repeat units. Overall, polymeric NFAs have not been as successful as their small molecule counterparts, mainly due to their suboptimal blend morphology. Their inherent polydispersity and batch-to-batch variations in molecular weight further complicate device optimisation thus directly impacting the PCE and reproducibility of the devices. If polymer acceptors are to become an industrial reality, these issues must first be tackled in order to exploit their remaining advantageous properties such as their excellent compatibility with industrial printing techniques.

5. Industrial considerations for NFAs

5.1. Synthetic complexity

The most highly cited metric in OPV research papers is the PCE of a given donor:acceptor combination. Whilst its importance in determining the industrial success of OPV materials should not be underestimated, additional factors such as the long-term stability and synthetic complexity of the materials employed are also critical. Previous publications have already been directed towards the cost analysis of OPV technologies, yielding an acceptable cost for commercially viable OPV modules of around 10 € g^{-1}.[123,124] Although the cost of fabricating a photovoltaic module entails different contributions, the primary driver arises from the material costs, in particular from the active layer materials.[125] The cost of the

Open Access Article. Published on 26 April 2018. Downloaded on 3/28/2024 5:48:32 PM.
This article is licensed under a Creative Commons Attribution 3.0 Unported Licence.

donor and acceptor employed is in turn primarily dependent on their synthetic accessibility, which broadly speaking is related to the number of synthetic steps (NSS) required.[126] Taking the acceptor's core as starting point, Tables S1–S5 (ESI†) detail the commercially available starting materials and NSS required for the various NFAs reported herein. One limitation of this approach is that acceptors featuring highly complex π-bridges and end groups will be favoured, as the additional synthetic complexity poised by these will not be considered. For a more detailed and complete account of the cost and synthetic evaluation of photovoltaic materials the reader is directed elsewhere.[123,125]

From the synthetic complexity data it follows that NFAs employing either fluorene, carbazole, PDI or NDI as their core appear to be more suited for industrial scale-up due to their relatively low NSS. Conversely, IDT and IDTT based acceptors appear to have a synthetic disadvantage due to the increased NSS (5–10) required to afford the target molecule. The primary cause for this drawback is the multistep synthesis of the as of yet commercial availability of IDT/IDTT cores; the issue of synthetic complexity is further compounded in IDT/IDTT based NFAs bearing pendant alkyl rather than aryl chains where three additional chemical transformations are required. Investment in scale-up and reverse engineering of the alkyl IDT may be offset by its prevalent use in charge transport polymers. The higher NSS of IDT/IDTT based NFAs is also largely offset by their superior OPV performance compared to other acceptors, thus effectively leading to a trade-off between synthetic complexity and photovoltaic performance. It is interesting to note that if the starting material for PDI based acceptors was to be synthesised from simpler chemical building blocks as shown in Fig. 15, the NSS required for PDI based acceptors would in theory be very similar compared to the IDT/IDTT based ones. This highlights the importance of developing commercially available intermediates to reduce the NSS and cost of producing electron acceptors.

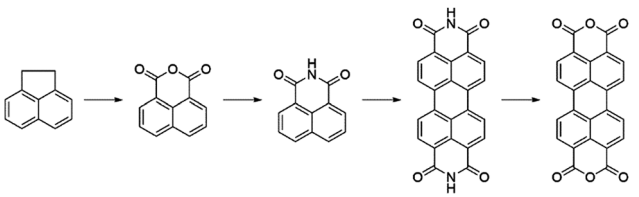

Fig. 15 Synthetic route employed for the synthesis of the starting material for PDI based acceptors.

5.2. Industrial printing techniques

Another key issue facing the commercialization of OPV, is the ability to produce devices with industrially scalable printing technologies. The need for non-halogenated solvent processing has been discussed above, however the technique used to deposit the active layer must also be considered. Spin-coating is an energy and material intensive printing technique that does not translate well to large scale production,[127] however it often produces the highest performance in small area devices for research purposes, and as such, it is used extensively in the device fabrication reported throughout OPV literature. For spin cast active layers the donor:acceptor ratio, solution concentration and solvent choice are optimized such that the aggregation of the donor and acceptor, which occurs as the solvent evaporates, lead to the formation nanoscale interpenetrating domains that are ideal in bulk heterojunctions. The issues presented by spin-coating include: (i) the large amount of active layer material ejected during the spinning of the substrate and (ii) the ability to only cast the active layer of one substrate at a time, rather than in a roll-to-roll (R2R) system.[128,129] Also spin coating is such a rapid kinetic process that the thermodynamically favoured phase separation processes are suppressed, leading to significant post-deposition morphology changes. Technologies such as slot-die coating and blade coating provide scalable alternatives to spin coating, and both of these technologies lend themselves well to large area R2R casting, allowing for a high throughput and more economically viable production process. The drying kinetics and aggregation of active layer solutions when blade or slot-die coating are rather different to those of spin coating, and thus require careful optimization of processing conditions, which are likely to differ from those used when spin coating.[130,131] Table 6 details a number of notable devices that have been produced using slot-die and blade coating to process the active layer. In general, lower PCEs are observed for R2R printed devices at present, however as more research efforts are directed towards tackling the problems of maintaining optimal morphology when using alternative printing techniques this gap is likely to close. In the three cases employing blade coating cited in Table 6, OPVs employing a similar donor:acceptor combination to their spin-coated correspondent yielded almost identical PCEs, highlighting the potential of this particular deposition method for large area organic solar cells. In the case of the FTAZ:**IT-M** and PBTA-TF:**IT-M** blends the use of relatively low boiling point solvents contributed towards the high PCEs observed. This is because the longer drying times associated with blade coating compared to spin coating can

Table 6 Summary of the *J*–*V* characteristics of different donor:NFA bulk heterojunction solar cells using various R2R printing techniques

Acceptor	V_{OC} (V)	J_{SC} (mA cm^{-2})	FF	PCE (%)	Donor	Coating technique	Ref.
IEIC	0.94	6.89	0.35	2.05	PTB7-Th	Slot-die	134
PNDIT	0.87	8.51	0.50	3.71	PII2T-PS	Slot-die	135
O-IDTBR	0.72	12.55	0.67	6.05	P3HT	Blade	136
IT-M	0.95	16.80	0.66	10.60	FTAZ	Blade	137
IT-M	0.95	18.14	0.66	11.40	PBTA-TF	Blade	138
$PC_{61}BM$	0.87	10.76	0.42	3.60	TQ1	Spray	139
$PC_{61}BM$	0.59	8.46	0.67	3.34	P3HT	Push	140

 This journal is © The Royal Society of Chemistry 2019

Open Access Article. Published on 26 April 2018. Downloaded on 3/28/2024 5:48:32 PM.
This article is licensed under a Creative Commons Attribution 3.0 Unported Licence.

be circumvented by the use of volatile processing solvents, thus enabling fast solvent evaporation and preventing large scale aggregation in the active layer of blade coated cells. The use of spray coating and push coating have also been reported in the fabrication of fullerene based devices.[132,133] The ability to produce devices that are able to achieve >3% PCE using both of these techniques suggest that they may also show promise as suitable alternatives in the production of large area devices.

6. Outlook & conclusions

To conclude, a plethora of design strategies have been utilized in the pursuit of developing a suitable replacement for the fullerene acceptors used in OPV, and as a result of much of the exciting work discussed in this review an explosion in the field of NFAs has occurred within the last 5 years. The dominance that NFAs have established in recent times can be illustrated by the number of NFA-based devices that now exceed the device performance achieved in the analogous fullerene-containing OSCs (see Table S6 and associated text in the ESI†).

Small molecule acceptors currently hold a significant advantage over their polymeric counterparts. The lack of entropic driving force for the polymeric acceptors to mix with a polymer donor has led to several reports of suboptimal morphologies, and thus limited PCEs in devices, although there are a small number of examples where promising efficiencies have been achieved in all-polymer solar cells. The batch-to-batch variations in molecular weight, PDI and regioregularity, currently observed in polymeric materials synthesized in sub gram quantities, leaves them at a disadvantage to small molecules, where batches will always be virtually identical. This inability to produce identical polymer batches on a regular basis provides an obvious impediment to the commercialization of polymeric NFAs. PDI based small molecule NFAs have made telling strides from the early reported acceptors, and by employing π-conjugated bridges and twisted 3D structures it has been possible to control the optoelectronic properties to maximize the V_{OC} in devices, and suppress the microscale aggregation that plagued early materials, resulting in vastly improved blend morphologies. Many of the PDI acceptors are relatively simple from a synthetic viewpoint, and are able to attain PCEs of >8.5% on a regular basis, yielding them exciting candidates to replace fullerenes. However, almost all of these acceptors require high-boiling halogenated additives in order to achieve the desired blend morphology; not only is it unlikely for these additives to be permitted in the printing industry, but they have also been shown to often cause morphological and photo-instability in OPV devices. Thus, developing PDIs with improved solubility and further suppression of aggregation should be of high priority to avoid the need of such additives, rendering them more feasible to use in OPV devices. Of all the classes of NFAs discussed in this work, A–D–A type acceptors appear to be the most attractive by some margin. The IDT and IDTT acceptors are now able to consistently achieve exceptional efficiencies of over 10% due to their high lying LUMOs, narrow bandgaps and controlled aggregation. Though PDIs may have a slight advantage in terms of synthetic simplicity, the A–D–A type acceptors can achieve higher PCEs, without the need for additives in several cases, and a number of highly stable devices have been reported. Additionally, the modular fashion in which the A–D–A acceptors are produced provides a number of opportunities to further tune these acceptors to maximize their performance. A large proportion of the recent success of OPV can be attributed to the quick and strategic evolution of non-fullerene acceptors, and they are likely to play a vital role in the future of organic solar cells as further improvements in their design are realized.

Table 7 Summary of the best performing NFAs and their corresponding properties in OPVs

Acceptor	PCE (%)	Donor	NSS	Additive
FDICTF[a]	10.06	PBDB-T	8	—
O-IDTBR[a,b]	6.38	P3HT	10	—
EH-IDTBR[a]	11.09	PffBT4T-2DT	10	—
ITIC[a]	11.34	PBQ-4F	5	5.0% IPA
ITIC-Th[a]	10.88	PTFB-O	5	—
IT-M[a,b]	12.05	PBDB-T	5	1.0% DIO
IT-4F[a]	13.10	PBDBT-SF	5	0.5% DIO
SF-PDI$_2$[a]	9.50	P3TEA	3	2.5% ODT
Ta-PDI[a]	9.15	PTB7-Th	4	—
P(NDI2OD-T2)[a]	10.10	PTz-BI-Si	3	—

[a] Fabricated by spin-coating. [b] Fabricated by blade-coating.

A number of the best performing NFAs have been summarized in Table 7, below. These acceptors are able to achieve amongst the highest efficiencies in their respective classes, whilst often possessing other advantageous features such as: (i) greater synthetic simplicity (**SF-PDI$_2$**, **Ta-PDI** and **P(NDI2OD-T2)**), (ii) the use of non-chlorinated solvent processing (**FDICTF**, **O-IDTBR**, **EH-IDTBR**, **Ta-PDI** and **P(NDI2OD-T2)**), (iii) a greater degree of flexibility in the donor polymers they can be paired with (**EH-IDTBR**, **ITIC**, **ITIC-Th** and **P(NDI2OD-T2)**) and (iv) the ability to process high efficiency devices with industrially viable deposition methods (**O-IDTBR** and **IT-M**). Though these acceptors are likely to form the basis for a considerable fraction of further development in the field of NFAs, the wide variety of design strategies and chemical moieties present in each of these acceptors indicates the large number of viable approaches to push the boundaries of NFA performance.

As a general note on the further development of NFAs, care must be taken that the pursuit of an ever-greater PCE does not become the sole point of focus. Through rational design there has been an enhancement in the performance of NFAs over time, however this is often accompanied by a substantial increase in the synthetic complexity of the acceptors or the need for unfavorable solvent systems in processing devices. Whilst this is often necessary to drive the development in this field, it should not outweigh the aims to produce cheap, scalable and highly stable devices, since the ultimate goal remains to be commercially viable OPV. As we approach 14–15% PCE with organic solar cells, the bottle neck in producing large scale OPV will become factors such as the cost and availability of the materials, compatibility with industrial printing processes and stability, rather than insufficient PCE to compete with rival technologies. Though there is some work currently being carried out on these

problems, at present there appears to be less value placed on them in academia than there is on chasing a record PCE, which could relegate the field of OPV to the realms of academic curiosity rather than an achievable renewable energy technology should this imbalance in the research persist.

Conflicts of interest

There are no conflicts to declare.

Acknowledgements

We acknowledge funding from KAUST and BASF, as well as EPSRC Project EP/G037515/1, EP/M005143/1, EC FP7 Project SC2 (610115), and EC H2020 Project SOLEDLIGHT (643791) for their financial support.

References

1 Y. He and Y. Li, *Phys. Chem. Chem. Phys.*, 2011, **13**, 1970–1983.
2 X. Yang, J. Loos, S. Veenstra, W. J. H. Verhees, M. M. Wienk, J. M. Kroon, M. Michels and R. A. J. Janssen, *Nano Lett.*, 2005, **5**, 579–583.
3 J. D. A. Lin, O. V. Mikhnenko, J. Chen, Z. Masri, A. Ruseckas, A. Mikhailovsky, R. P. Raab, J. Liu, P. W. M. Blom, M. A. Loi, C. J. Garcia-Cervera, I. W. Samuel and T. Q. Nguyen, *Mater. Horiz.*, 2014, **1**, 280–285.
4 Y. Tamai, H. Ohkita, H. Benten and S. Ito, *J. Phys. Chem. Lett.*, 2015, **6**, 3417–3428.
5 M. M. Wienk, J. M. Kroon, W. J. H. Verhees, J. Knol, J. C. Hummelen, P. A. van Hal and R. A. J. Janssen, *Angew. Chem., Int. Ed.*, 2003, **42**, 3371–3375.
6 F. B. Kooistra, J. Knol, F. Kastenberg, L. M. Popescu, W. J. H. Verhees, J. M. Kroon and J. C. Hummelen, *Org. Lett.*, 2007, **9**, 551–554.
7 M. Lenes, G. J. A. H. Wetzelaer, F. B. Kooistra, S. C. Veenstra, J. C. Hummelen and P. W. M. Blom, *Adv. Mater.*, 2008, **20**, 2116–2119.
8 C. Z. Li, S. C. Chien, H. L. Yip, C. C. Chueh, F. C. Chen, Y. Matsuo, E. Nakamura and A. K. Y. Jen, *Chem. Commun.*, 2011, **47**, 10082–10084.
9 Y. He, H. Y. Chen, J. Hou and Y. Li, *J. Am. Chem. Soc.*, 2010, **132**, 1377–1382.
10 M. Campoy-Quiles, T. Ferenczi, T. Agostinelli, P. G. Etchegoin, Y. Kim, T. D. Anthopoulos, P. N. Stavrinou, D. D. C. Bradley and J. Nelson, *Nat. Mater.*, 2008, **7**, 158–164.
11 S. R. Dupont, M. Oliver, F. C. Krebs and R. H. Dauskardt, *Sol. Energy Mater. Sol. Cells*, 2012, **97**, 171–175.
12 B. J. T. de Villers, K. A. O'Hara, D. P. Ostrowski, P. H. Biddle, S. E. Shaheen, M. L. Chabinyc, D. C. Olson and N. Kopidakis, *Chem. Mater.*, 2016, **28**, 876–884.
13 W. Chen and Q. Zhang, *J. Mater. Chem. C*, 2017, **5**, 1275–1302.
14 Z. He, B. Xiao, F. Liu, Y. Yang, S. Xiao, C. Wang, T. P. Russell and Y. Cao, *Nat. Photonics*, 2015, **9**, 174–179.
15 Y. Liu, J. Zhao, Z. Li, C. Mu, W. Ma, H. Hu, K. Kiang, H. Lin, H. Ade and H. Yan, *Nat. Commun.*, 2014, **5**, 5293.
16 T. Ameri, J. Min, N. Li, F. Machui, D. Baran, M. Forster, K. J. Schottler, D. Dolfen, U. Scherf and C. J. Brabec, *Adv. Energy Mater.*, 2012, **2**, 1198–1202.
17 L. Lu, T. Xu, W. Chen, E. S. Landry and L. Yu, *Nat. Photonics*, 2014, **8**, 716–722.
18 P. P. Khlyabich, B. Burkhart and B. C. Thompson, *J. Am. Chem. Soc.*, 2011, **133**, 14534–14537.
19 J. Zhang, Y. Zhang, J. Fang, K. Lu, Z. Wang, W. Ma and Z. Wei, *J. Am. Chem. Soc.*, 2015, **137**, 8176–8183.
20 B. J. Kim, Y. Miyamoto, B. Ma and J. M. J. Fréchet, *Adv. Funct. Mater.*, 2009, **19**, 2273–2281.
21 J. E. Carlé, B. Andreasen, T. Tromholt, M. V. Madsen, K. Norman, M. Jørgensen and F. C. Krebs, *J. Mater. Chem.*, 2012, **22**, 24417–24423.
22 J. W. Rumer, R. S. Ashraf, N. D. Eisenmenger, Z. Huang, I. Meager, C. B. Nielsen, B. C. Schroeder, M. L. Chabinyc and I. McCulloch, *Adv. Energy Mater.*, 2015, **5**, 1401426.
23 J. W. Rumer and I. McCulloch, *Mater. Today*, 2015, **8**, 425–435.
24 J. Zhao, Y. Li, G. Yang, K. Jiang, H. Lin, H. Ade, W. Ma and H. Yan, *Nat. Energy*, 2016, **1**, 15027.
25 Z. Xu, L. M. Chen, G. Yang, C. H. Huang, J. Hou, Y. Wu, G. Li, C. S. Hsu and Y. Yang, *Adv. Funct. Mater.*, 2009, **19**, 1227–1234.
26 Y. Yan, Z. Liu and T. Wang, *Adv. Mater.*, 2017, **29**, 1601674.
27 J. R. Tumbleston, D. H. Ko, E. T. Samulski and R. Lopez, *Phys. Rev. B: Condens. Matter Mater. Phys.*, 2010, **82**, 205325.
28 T. J. K. Brenner, Y. Vaynzof, Z. Li, D. Kabra, R. H. Friend and C. R. McNeill, *J. Phys. D: Appl. Phys.*, 2012, **45**, 415101.
29 I. Etxebarria, A. Guerrero, J. Alberto, G. Garcia-Belmonte, E. Palomares and R. Pacios, *Org. Electron.*, 2014, **15**, 2756–2762.
30 K. Cnops, B. P. Rand, D. Cheyns, B. Verreet, M. A. Empl and P. Heremans, *Nat. Commun.*, 2014, **5**, 3406.
31 K. Cnops, G. Zango, J. Genoe, P. Heremans, M. V. Martinez-Diaz, T. Torres and D. Cheyns, *J. Am. Chem. Soc.*, 2015, **137**, 8991–8997.
32 B. Ebenhoch, N. B. A. Prasetya, V. M. Rotello, G. Cooke and I. D. W. Samuel, *J. Mater. Chem. A*, 2015, **3**, 7345–7352.
33 C. B. Nielsen, E. Voroshazi, S. Holliday, K. Cnops, B. P. Rand and I. McCulloch, *J. Mater. Chem. A*, 2013, **1**, 73.
34 C. B. Nielsen, E. Voroshazi, S. Holliday, K. Cnops, D. Cheyns and I. McCulloch, *J. Mater. Chem. A*, 2014, **2**, 12348–12354.
35 G. Zhang, V. Lami, F. Rominger, Y. Vaynzof and M. Mastalerz, *Angew. Chem., Int. Ed.*, 2016, **55**, 3977–3981.
36 Y. Kim, C. E. Song, S.-J. Moon and E. Lim, *Chem. Commun.*, 2014, **50**, 8235–8238.
37 H. Shi, W. Fu, M. Shi, J. Ling and H. Chen, *J. Mater. Chem. A*, 2015, **3**, 1902–1905.
38 S. Holliday, R. S. Ashraf, C. B. Nielsen, M. Kirkus, J. A. Röhr, C.-H. Tan, E. Collado-Fregoso, A.-C. Knall, J. R. Durrant, J. Nelson and I. McCulloch, *J. Am. Chem. Soc.*, 2015, **137**, 898–904.
39 D. Baran, T. Kirchartz, S. Wheeler, S. Dimitrov, M. Abdelsamie, J. Gorman, R. S. Ashraf, S. Holliday,

Open Access Article. Published on 26 April 2018. Downloaded on 3/28/2024 5:48:32 PM. This article is licensed under a Creative Commons Attribution 3.0 Unported Licence.

Open Access Article. Published on 26 April 2018. Downloaded on 3/28/2024 5:48:32 PM.
This article is licensed under a Creative Commons Attribution 3.0 Unported Licence.

A. Wadsworth, N. Gasparini, P. Kaienburg, H. Yan, A. Amassian, C. J. Brabec, J. R. Durrant and I. McCulloch, *Energy Environ. Sci.*, 2016, **9**, 3783–3793.
40 M. Li, Y. Liu, W. Ni, F. Liu, H. Feng, Y. Zhang, T. Liu, H. Zhang, X. Wan, B. Kan, Q. Zhang, T. P. Russell and Y. Chen, *J. Mater. Chem. A*, 2016, **4**, 10409–10413.
41 N. Qiu, H. Zhang, X. Wan, C. Li, X. Ke, H. Feng, B. Kan, H. Zhang, Q. Zhang, Y. Lu and Y. Chen, *Adv. Mater.*, 2017, **29**, 1604964.
42 K. Wang, Y. Firdaus, M. Babics, F. Cruciani, Q. Saleem, A. El Labban, M. A. Alamoudi, T. Marszalek, W. Pisula, F. Laquai and P. M. Beaujuge, *Chem. Mater.*, 2016, **28**, 2200–2208.
43 N. Qiu, X. Yang, H. Zhang, X. Wan, C. Li, F. Liu, H. Zhang, T. P. Russell and Y. Chen, *Chem. Mater.*, 2016, **28**, 6770–6778.
44 A. Gupta, A. Rananaware, P. S. Rao, D. D. La, A. Bilic, W. Xiang, J. Li, R. A. Evans, S. V. Bhosale and S. V. Bhosale, *Mater. Chem. Front.*, 2017, **1**, 1600–1606.
45 Y. Lin, Z.-G. Zhang, H. Bai, J. Wang, Y. Yao, Y. Li, D. Zhu and X. Zhan, *Energy Environ. Sci.*, 2015, **8**, 610–616.
46 H. Lin, S. Chen, Z. Li, J. Y. L. Lai, G. Yang, T. McAfee, K. Jiang, Y. Li, Y. Liu, H. Hu, J. Zhao, W. Ma, H. Ade and H. Yan, *Adv. Mater.*, 2015, **27**, 7299–7304.
47 H. Yao, Y. Chen, Y. Qin, R. Yu, Y. Cui, B. Yang, S. Li, K. Zhang and J. Hou, *Adv. Mater.*, 2016, **28**, 8283–8287.
48 Y. Li, L. Zhong, F.-P. Wu, Y. Yuan, H.-J. Bin, Z.-Q. Jiang, Z. Zhang, Z.-G. Zhang, Y. Li and L.-S. Liao, *Energy Environ. Sci.*, 2016, **9**, 3429–3435.
49 S. Holliday, R. S. Ashraf, A. Wadsworth, D. Baran, S. A. Yousaf, C. B. Nielsen, C.-H. Tan, S. D. Dimitrov, Z. Shang, N. Gasparini, M. Alamoudi, F. Laquai, C. J. Brabec, A. Salleo, J. R. Durrant and I. McCulloch, *Nat. Commun.*, 2016, **7**, 11585.
50 D. Baran, R. S. Ashraf, D. A. Hanifi, M. Abdelsamie, N. Gasparini, J. A. Röhr, S. Holliday, A. Wadsworth, S. Lockett, M. Neophytou, C. J. M. Emmott, J. Nelson, C. J. Brabec, A. Amassian, A. Salleo, T. Kirchartz, J. R. Durrant and I. McCulloch, *Nat. Mater.*, 2017, **16**, 363–369.
51 A. Wadsworth, R. S. Ashraf, M. Abdelsamie, S. Pont, M. Little, M. Moser, Z. Hamid, M. Neophytou, W. Zhang, A. Amassian, J. R. Durrant, D. Baran and I. McCulloch, *ACS Energy Lett.*, 2017, **2**, 1494–1500.
52 Y. Wu, H. Bai, Z. Wang, P. Cheng, S. Zhu, Y. Wang, W. Ma and X. Zhan, *Energy Environ. Sci.*, 2015, **8**, 3215–3221.
53 Q.-Y. Li, J. Xiao, L.-M. Tang, H.-C. Wang, Z. Chen, Z. Yang, H.-L. Yip and Y.-X. Xu, *Org. Electron.*, 2017, **44**, 217–224.
54 B. Jia, Y. Wu, F. Zhao, C. Yan, S. Zhu, P. Cheng, J. Mai, T. K. Lau, X. Lu, C. J. Su, C. Wang and X. Zhan, *Sci. China: Chem.*, 2017, **60**, 257–263.
55 F. Liu, Z. Zhou, C. Zhang, T. Vergote, H. Fan, F. Liu and X. Zhu, *J. Am. Chem. Soc.*, 2016, **138**, 15523–15526.
56 Y. Lin, J. Wang, Z.-G. Zhang, H. Bai, Y. Li, D. Zhu and X. Zhan, *Adv. Mater.*, 2015, **27**, 1170–1174.
57 Z. Zheng, O. M. Awartani, B. Gautam, D. Liu, Y. Qin, W. Li, A. Bataller, K. Gundogdu, H. Ade and J. Hou, *Adv. Mater.*, 2017, **29**, 1604241.
58 Y. Lin, F. Zhao, Q. He, L. Huo, Y. Wu, T. C. Parker, W. Ma, Y. Sun, C. Wang, D. Zhu, A. J. Heeger, S. R. Marder and X. Zhan, *J. Am. Chem. Soc.*, 2016, **138**, 4955–4961.
59 L. Chang, H. W. A. Lademann, J. B. Bonekamp, M. Meerholz and A. J. Moulé, *Adv. Funct. Mater.*, 2011, **21**, 1779–1787.
60 Z. Li, K. Jiang, G. Yang, J. Y. L. Lai, T. Ma, J. Zhao, W. Ma and H. Yan, *Nat. Commun.*, 2016, **7**, 13094.
61 Y. Lin, Q. He, F. Zhao, L. Huo, J. Mai, X. Lu, C.-J. Su, T. Li, J. Wang, J. Zhu, Y. Sun, C. Wang and X. Zhan, *J. Am. Chem. Soc.*, 2016, **138**, 2973–2976.
62 S. Li, L. Ye, W. Zhao, S. Zhang, S. Mukherjee, H. Ade and J. Hou, *Adv. Mater.*, 2016, **28**, 9423–9429.
63 W. Zhao, D. Qian, S. Zhang, S. Li, O. Inganäs, F. Gao and J. Hou, *Adv. Mater.*, 2016, **28**, 4734–4739.
64 W. Zhao, S. Li, H. Yao, S. Zhang, Y. Zhang, B. Yang and J. Hou, *J. Am. Chem. Soc.*, 2017, **139**, 7148–7151.
65 K. Reichenbacher, H. I. Suss and J. Hulliger, *Chem. Soc. Rev.*, 2005, **34**, 22–30.
66 Y. Yang, Z.-G. Zhang, H. Bin, S. Chen, L. Gao, L. Xue, C. Yang and Y. Li, *J. Am. Chem. Soc.*, 2016, **138**, 15011–15018.
67 Y. Li, L. Zhong, B. Gautam, H.-J. Bin, J.-D. Lin, F.-P. Wu, Z. Zhang, Z.-Q. Jiang, Z.-G. Zhang, K. Gundogdu, Y. Li and L.-S. Liao, *Energy Environ. Sci.*, 2017, **10**, 1610–1620.
68 X. Zhan, A. Facchetti, S. Barlow, T. J. Marks, M. A. Ratner, M. R. Wasielewski and S. R. Marder, *Adv. Mater.*, 2011, **23**, 268–284.
69 C. B. Nielsen, S. Holliday, H.-Y. Chen, S. J. Cryer and I. McCulloch, *Acc. Chem. Res.*, 2015, **48**, 2803–2812.
70 F. Würthner, *Chem. Commun.*, 2004, 1564–1579.
71 W. Zhang, J. Smith, S. E. Watkins, R. Gysel, M. McGehee, A. Salleo, J. Kirkpatrick, S. Ashraf, T. Anthopoulos, M. Heeney and I. McCulloch, *J. Am. Chem. Soc.*, 2010, **132**, 11437–11439.
72 C. L. Zhan and A. D. Q. Li, *Curr. Org. Chem.*, 2011, **15**, 1314–1339.
73 A. Sharenko, C. M. Proctor, T. S. van der Poll, Z. B. Henson, T.-Q. Nguyen and G. C. Bazan, *Adv. Mater.*, 2013, **25**, 4403–4407.
74 Y. X. Chen, X. Zhang, C. L. Zhan and J. N. Yao, *Phys. Status Solidi A*, 2015, **212**, 1961–1968.
75 R. Shivanna, S. Shoaee, S. Dimitrov, S. K. Kandappa, S. Rajaram, J. R. Durrant and K. S. Narayan, *Energy Environ. Sci.*, 2014, **7**, 435–441.
76 C.-H. Wu, C.-C. Chueh, Y.-Y. Xi, H.-L. Zhong, G.-P. Gao, Z.-H. Wang, L. D. Pozzo, T.-C. Wen and A. K.-Y. Jen, *Adv. Funct. Mater.*, 2015, **25**, 5326–5332.
77 W. Jiang, L. Ye, X. Li, X. Ciao, F. Tan, W. Zhao, J. Hou and Z. Wang, *Chem. Commun.*, 2014, **50**, 1024–1026.
78 L. Ye, W. Jiang, W. Zhao, S. Zhang, D. Qian, Z. Wang and J. Hou, *Small*, 2014, **10**, 4658–4663.
79 Y. Zang, C.-Z. Li, C.-C. Chueh, S. T. Williams, W. Jiang, Z.-H. Wang, J.-S. Yu and A. K.-Y. Jen, *Adv. Mater.*, 2014, **26**, 5708–5714.
80 D. Sun, D. Meng, Y. Cai, B. Fan, Y. Li, W. Jiang, L. Huo, Y. Sun and Z. Wang, *J. Am. Chem. Soc.*, 2015, **137**, 11156–11162.
81 D. Meng, D. Sun, C. Zhong, T. Liu, B. Fan, L. Huo, Y. Li, W. Jiang, H. Choi, T. Kim, J. Y. Kim, Y. Sun, Z. Wang and A. J. Heeger, *J. Am. Chem. Soc.*, 2016, **138**, 375–380.

Open Access Article. Published on 26 April 2018. Downloaded on 3/28/2024 5:48:32 PM.
This article is licensed under a Creative Commons Attribution 3.0 Unported Licence.

82 Y. Zhong, M. T. Trinh, R. Chen, W. Wang, P. P. Khlyabich, B. Kumar, Q. Xu, C.-Y. Nam, M. Y. Sfeir, C. Black, M. L. Steigerwald, Y.-L. Loo, S. Xiao, F. Ng, X. Y. Zhu and C. Nuckolls, *J. Am. Chem. Soc.*, 2014, **136**, 15215–15221.
83 X. Zhang, Z. Lu, L. Ye, C. Zhan, J. Hou, S. Zhang, B. Jiang, Y. Zhao, J. Huang, S. Zhang, Y. Liu, Q. Shi, Y. Liu and J. Yao, *Adv. Mater.*, 2013, **25**, 5791–5797.
84 X. Zhang, C. Zhan and J. Yao, *Chem. Mater.*, 2015, **27**, 166–173.
85 X. Zhang, W. Li, J. Yao and C. Zhan, *ACS Appl. Mater. Interfaces*, 2016, **8**, 15415–15421.
86 B. Jiang, X. Zhang, Y. Zheng, G. Yu, J. Yao and C. Zhan, *RSC Adv.*, 2016, **6**, 43715–43718.
87 H. Zhong, C.-H. Wu, C.-Z. Li, J. Carpenter, C.-C. Chueh, J.-Y. Chen, H. Ade and A. K.-Y. Jen, *Adv. Mater.*, 2016, **28**, 951–958.
88 S. Li, W. Liu, C.-Z. Li, T.-K. Lau, X. Lu, M. Shi and H. Chen, *J. Mater. Chem. A*, 2016, **4**, 14983–14987.
89 J. Zhao, Y. Li, H. Lin, Y. Liu, K. Jiang, C. Mu, T. Ma, J. Y. Lin Lai, H. Hu, D. Yu and H. Yan, *Energy Environ. Sci.*, 2015, **8**, 520–525.
90 J. Liu, S. Chen, D. Qian, B. Gautam, G. Yang, J. Zhao, J. Bergqvist, F. Zhang, W. Ma, H. Ade, O. Inganäs, K. Gundogdu, F. Gao and H. Yan, *Nat. Energy*, 2016, **1**, 16089.
91 Y. Lin, Y. Wang, J. Wang, J. Hou, Y. Li, D. Zhu and X. Zhan, *Adv. Mater.*, 2014, **26**, 5137–5142.
92 S. Li, W. Liu, C.-Z. Li, F. Liu, Y. Zhang, M. Shi, H. Chen and T. P. Russell, *J. Mater. Chem. A*, 2016, **4**, 10659–10665.
93 D. Meng, H. Fu, C. Xiao, X. Meng, T. Winands, W. Ma, W. Wei, B. Fan, L. Huo, N. L. Doltsinis, Y. Li, Y. Sun and Z. Wang, *J. Am. Chem. Soc.*, 2016, **138**, 10184–10190.
94 Y. Duan, X. Xu, H. Yan, W. Wu, Z. Li and Q. Peng, *Adv. Mater.*, 2017, **29**, 1605115.
95 N. Liang, K. Sun, Z. Zheng, H. Yao, G. Gao, X. Meng, Z. Wang, W. Ma and J. Hou, *Adv. Energy Mater.*, 2016, **6**, 1600060.
96 Y. Zhong, M. T. Trinh, R. Chen, G. E. Purdum, P. P. Khlyabich, M. Sezen, S. Oh, H. Zhu, B. Fowler, B. Zhang, W. Wang, C.-Y. Nam, M. Y. Sfeir, C. T. Black, M. L. Steigerwald, Y.-L. Loo, F. Ng, X. Y. Zhu and C. Nuckolls, *Nat. Commun.*, 2015, **6**, 8242.
97 Y. Liu, C. Mu, K. Jiang, J. Zhao, Y. Li, L. Zhang, Z. Li, J. Y. L. Lai, H. Hu, T. Ma, R. Hu, D. Yu, X. Huang, B. Z. Tang and H. Yan, *Adv. Mater.*, 2015, **27**, 1015–1020.
98 H. Lin, S. Chen, H. Hu, L. Zhang, T. Ma, J. Y. L. Lai, Z. Li, A. Qin, X. Huang, B. Tang and H. Yan, *Adv. Mater.*, 2016, **28**, 8546–8551.
99 Q. Wu, D. Zhao, A. M. Schneider, W. Chen and L. Yu, *J. Am. Chem. Soc.*, 2016, **138**, 7248–7251.
100 J. J. Halls, C. A. Walsh, N. C. Greenham, E. A. Marseglia, R. H. Friend, S. C. Moratti and A. B. Holmes, *Nature*, 1995, **376**, 498–500.
101 H. Yan, Z. Chen, Y. Zheng, C. Newman, J. R. Quinn, F. Dötz, M. Kastler and A. Facchetti, *Nature*, 2009, **457**, 679–686.
102 J. R. Moore, S. Albert-Seifried, A. Rao, S. Massip, B. Watts, D. J. Morgan, R. H. Friend, C. R. McNeill and H. Sirringhaus, *Adv. Energy Mater.*, 2011, **1**, 230–240.
103 T. W. Holcombe, J. E. Norton, J. Rivnay, C. H. Woo, L. Goris, C. Piliego, G. Griffini, A. Sellinger, J.-L. Brédas, A. Salleo and J. M. J. Fréchet, *J. Am. Chem. Soc.*, 2011, **133**, 12106–12114.
104 M. Schubert, D. Dolfen, J. Frisch, S. Roland, R. Steyrleuthner, B. Stiller, Z. Chen, U. Scherf, N. Koch, A. Facchetti and D. Neher, *Adv. Energy Mater.*, 2012, **2**, 369–380.
105 D. Mori, H. Benten, I. Okada, H. Ohkita and S. Ito, *Adv. Energy Mater.*, 2014, **4**, 1301006.
106 L. Gao, Z.-G. Zhang, L. Xue, J. Min, J. Zhang, Z. Wei and Y. Li, *Adv. Mater.*, 2016, **28**, 1884–1890.
107 B. Fan, L. Ying, P. Zhu, F. Pan, F. Liu, J. Chen, F. Huang and Y. Cao, *Adv. Mater.*, 2017, **29**, 1703906.
108 W. Lee, C. Lee, H. Yu, D.-J. Kim, C. Wang, H. Y. Woo, J. H. Oh and B. J. Kim, *Adv. Funct. Mater.*, 2016, **26**, 1543–1553.
109 X. Wu, Y. Tang, Y. Wang, X. Liu, C. Liu, X. Zhang, Y. Yang, X. Gao, F. Chen, X. Guo and Z.-K. Chen, *J. Polym. Sci., Part A: Polym. Chem.*, 2017, **55**, 3679–3689.
110 J. W. Jung, J. W. Jo, C.-C. Chueh, F. Liu, W. H. Jo, T. P. Russell and A. K.-Y. Jen, *Adv. Mater.*, 2015, **27**, 3310–3317.
111 T. Kim, J. H. Kim, T. E. Kang, C. Lee, H. Kang, M. Shin, C. Wang, B. Ma, U. Jeong, T. S. Kim and B. J. Kim, *Nat. Commun.*, 2015, **6**, 8547.
112 T. Earmme, Y.-J. Hwang, N. M. Murari, S. Subramaniyan and S. A. Jenekhe, *J. Am. Chem. Soc.*, 2013, **135**, 14960–14963.
113 Y.-J. Hwang, B. A. E. Courtright, A. S. Ferreira, S. H. Tolbert and S. A. Jenehke, *Adv. Mater.*, 2015, **27**, 4578–4584.
114 L. Xue, Y. Yang, Z.-G. Zhang, X. Dong, L. Gao, H. Bin, J. Zhang, Y.-X. Yang and Y. Li, *J. Mater. Chem. A*, 2016, **4**, 5810–5816.
115 Y. Zhou, K. L. Gu, X. Gu, T. Kurosawa, H. Yan, Y. Guo, G. I. Koleilat, D. Zhao, M. F. Toney and Z. Bao, *Chem. Mater.*, 2016, **28**, 5037–5042.
116 S. Li, H. Zhang, W. Zhao, L. Ye, H. Yao, B. Yang, S. Zhang and J. Hou, *Adv. Energy Mater.*, 2016, **6**, 1–9.
117 Y. Guo, Y. Li, O. Awartani, J. Zhao, H. Han, H. Ade, D. Zhao and H. Yan, *Adv. Mater.*, 2016, **28**, 8483–8489.
118 Y. Guo, Y. Li, O. Awartani, H. Han, J. Zhao, H. Ade, H. Yan and D. Zhao, *Adv. Mater.*, 2017, **29**, 1700309.
119 M. Liu, J. Yang, C. Lang, Y. Zhang, E. Zhou, Z. Liu, F. Guo and L. Zhao, *Macromolecules*, 2017, **50**, 7559–7566.
120 Z. Li, W. Zhang, X. Xu, Z. Genene, D. Di Carlo Rasi, W. Mammo, A. Yartsev, M. R. Andersson, R. A. J. Janssen and E. Wang, *Adv. Energy Mater.*, 2017, **7**, 1602722.
121 Z. Li, X. Xu, W. Zhang, X. Meng, W. Ma, A. Yartsev, O. Inganäs, M. R. Andersson, R. A. J. Janssen and E. Wang, *J. Am. Chem. Soc.*, 2016, **138**, 10935–10944.
122 Y. J. Hwang, T. Earmme, B. A. E. Courtright, F. N. Eberle and S. A. Jenekhe, *J. Am. Chem. Soc.*, 2015, **137**, 4424–4434.
123 F. Machui, M. Hösel, N. Li, G. D. Spyropoulos, T. Ameri, R. R. Sondergaard, M. Jorgensen, A. Scheel, D. Gaiser, K. Kreul, D. Lenssen, M. Legros, N. Lemaitre, M. Vilkman, M. Välimäki, S. Nordman, C. J. Brabec and F. C. Krebs, *Energy Environ. Sci.*, 2014, **7**, 2792–2802.

 This journal is © The Royal Society of Chemistry 2019

Open Access Article. Published on 26 April 2018. Downloaded on 3/28/2024 5:48:32 PM.
This article is licensed under a Creative Commons Attribution 3.0 Unported Licence.

124 L. Lucera, P. Kubis, F. W. Fecher, C. Bronnbauer, M. Turbiez, K. Forberich, T. Ameri, H.-J. Egelhaaf and C. J. Brabec, *Energy Technol.*, 2015, **3**, 373–384.
125 J. Min, Y. N. Luponosov, C. Cui, B. Kan, H. Chen, X. Wan, Y. Chen, S. A. Ponomarenko, Y. Li and C. J. Brabec, *Adv. Energy Mater.*, 2017, **7**, 1700465.
126 E. Bundgaard, F. Livi, O. Hagemann, J. E. Carlé, M. Helgesen, I. M. Heckler, N. K. Zawacka, D. Angmo, T. T. Larsen-Olsen, G. A. dos Reitos Benatto, B. Roth, M. V. Madsen, M. R. Andersson, M. Jorgensen, R. R. Sondergaard and F. C. Krebs, *Adv. Energy Mater.*, 2015, **5**, 1402186.
127 A. Teichler, J. Perelaer and U. S. Schubert, *J. Mater. Chem. C*, 2013, **1**, 1910–1925.
128 R. R. Sondergaard, M. Hösel and F. C. Krebs, *J. Polym. Sci., Part B: Polym. Phys.*, 2013, **51**, 16–34.
129 F. C. Krebs, *Sol. Energy Mater. Sol. Cells*, 2009, **93**, 394–412.
130 R. Mens, P. Adriaensens, L. Lutsen, A. Swinnen, S. Bertho, B. Ruttens, J. D'Haen, J. Manca, T. Cleij, D. Vanderzande and J. Gelan, *J. Polym. Sci., Part A: Polym. Chem.*, 2008, **46**, 138–145.
131 B. Schmidt-Hansberg, M. F. G. Klein, K. Peters, F. Buss, J. Pfeifer, S. Wahlheim, A. Colsmann, U. Lemmer, P. Scharfer and W. Schabel, *J. Appl. Phys.*, 2009, **106**, 124501.
132 T. Wang, N. W. Scarratt, H. Yi, A. D. F. Dunbar, A. J. Pearson, D. C. Watters, T. S. Glen, A. C. Brook, J. Kinglsey, A. R. Buckley, M. W. A. Skoda, A. M. Donald, R. A. L. Jones, A. Iraqi and D. G. Lidzey, *Adv. Energy Mater.*, 2013, **3**, 505–512.
133 G. Susanna, L. Salamandra, T. M. Brown, A. Di Carlo, F. Brunetti and A. Reale, *Sol. Energy Mater. Sol. Cells*, 2011, **95**, 1775–1778.
134 K. Liu, T. T. Larsen-Olsen, Y. Lin, M. Beliatis, E. Bundgaard, M. Jørgensen, F. C. Krebs and X. Zhan, *J. Mater. Chem. A*, 2016, **4**, 1044–1051.
135 X. Gu, Y. Zhou, K. Gu, T. Kurosawa, Y. Guo, Y. Li, H. Lin, B. C. Schroeder, H. Yan, F. Molina-Lopez, C. J. Tassone, C. Wang, S. C. B. Mannsfeld, H. Yan, D. Zhou, M. F. Toney and Z. Bao, *Adv. Energy Mater.*, 2017, **7**, 1602742.
136 N. Gasparini, M. Salvador, S. Strohm, T. Heumueller, I. Levchuk, A. Wadsworth, J. H. Bannock, J. C. de Mello, H. Egelhaaf, D. Baran, I. McCulloch and C. J. Brabec, *Adv. Energy Mater.*, 2017, **7**, 1700770.
137 L. Ye, Y. Xiong, Q. Zhang, S. Li, C. Wang, Z. Jiang, J. Hou, W. You and H. Ade, *Adv. Mater.*, 2018, **30**, 1705485.
138 W. Zhao, S. Zhang, Y. Zhang, S. Li, X. Liu, C. He, Z. Zheng and J. Hou, *Adv. Mater.*, 2018, **30**, 1704837.
139 C. Cai, Y. Zhang, R. Song, Z. Peng, L. Xia, M. Wu, K. Xiong, B. Wang, Y. Lin, X. Xu, Q. Liang, H. Wu, E. Wang and L. Hou, *Sol. Energy Mater. Sol. Cells*, 2017, **161**, 52–61.
140 V. Vohra, W. Mróz, S. Inaba, W. Porzio, U. Giovanella and F. Galeotti, *ACS Appl. Mater. Interfaces*, 2017, **9**, 25434–25444.